AN ANALYTICAL EVALUATION OF DISTORTION-INDUCED FATIGUE IN STEEL BRIDGES

BY

Heidi L. Hassel

Submitted to the graduate degree program in Civil, Architectural, and Environmental Engineering and the Graduate Faculty of the University of Kansas in partial fulfillment of the requirements for the degree of Master's of Science.

Committee members: _____
Chairperson Dr. Caroline Bennett

_____
Dr. Adolfo Matamoros

_____
Dr. Stanley Rolfe

Date defended: January 28, 2011

The Thesis Committee for Heidi L. Hassel
certifies that this is the approved Version of the following thesis:

**AN ANALYTICAL EVALUATION OF
DISTORTION-INDUCED FATIGUE IN STEEL BRIDGES**

Committee members: _____
Chairperson Dr. Caroline Bennett

_____
Dr. Adolfo Matamoros

_____
Dr. Stanley Rolfe

Date approved: _____

EXECUTIVE SUMMARY

Multi-girder steel bridges designed prior to the mid-1980's, have developed cracks due to distortion-induced fatigue. An analytical evaluation was conducted to better understand the effects of bridge configurations and common retrofits on distortion-induced fatigue, as quantified by hot spot stress in web gap regions. Results are described herein and present relative distortion-induced fatigue susceptibility of multi-girder bridges with varied skew angle, cross frame spacing, bracing configuration, and cross frame stiffness as well as regions within each variation where cracking is most likely to occur. Performance of retrofit techniques was also compared and included positive attachment, a slotted connection stiffener, a back-up stiffener, and cross frame removal with each implemented both locally and globally. In addition, influence surfaces were generated and analyzed for three bridge configurations to better understand the relationship between load placement and distortion-induced fatigue related stresses. It is hoped that this research will benefit bridge engineers working to identify and extend the fatigue life of bridges susceptible to distortion-induced fatigue.

This paper is organized into two primary parts. The first, entitled "Distortion-Induced Fatigue in Steel Bridges: Causes, Parameters, and Fixes" is a stand-alone article and was published in the conference proceedings of the American Society of Civil Engineers/Structural Engineering Institute (ASCE/SEI) Structures Congress, held in Orlando, Florida in May 2010. The second is entitled "Parametric Analysis of Cross Frame Configuration on Distortion-Induced Fatigue in Skewed Steel Bridges." The main body of the second portion is intended for future publication and therefore, supplementary material containing additional details of the investigation have been included in appendices and are separated by topic.

ACKNOWLEDGEMENTS

It is a pleasure to thank those who made this thesis possible. This report would not have been possible without the guidance, support, and expertise of Drs. Caroline Bennett, Adolfo Matamoros, and Stanley Rolfe. In addition, I would like to thank my colleagues for their assistance, especially Amanda Hartman and Say Hak Bun. I would like to gratefully acknowledge support of the Kansas Department of Transportation (KDOT), University of Kansas Transportation Research Institute (KU TRI), and Transportation Pooled Fund Study TPF-T(189). Finally, I would like to thank my husband for his support and encouragement.

TABLE OF CONTENTS

PART 1: DISTORTION-INDUCED FATIGUE IN STEEL BRIDGES: CAUSES, PARAMETERS, AND FIXES

PART 2: PARAMETRIC ANALYSIS OF CROSS FRAME CONFIGURATION ON DISTORTION-INDUCED FATIGUE IN SKEWED STEEL BRIDGES

APPENDIX A: CROSS FRAME STIFFNESS WITH RESPECT TO DISTORTION-INDUCED FATIGUE

APPENDIX B: EFFECT OF WEB GAP LENGTH OF FATIGUE SUSCEPTIBILITY

APPENDIX C: INFLUENCE SURFACES RELATING LOAD PLACEMENT AND WEB GAP STRESSES

APPENDIX D: A DETAILED LOOK AT WEB GAP STRESSES

LIST OF TABLES

PART 1: DISTORTION-INDUCED FATIGUE IN STEEL BRIDGES: CAUSES, PARAMETERS, AND FIXES

PART 2: PARAMETRIC ANALYSIS OF CROSS FRAME CONFIGURATION ON DISTORTION-INDUCED FATIGUE IN SKEWED STEEL BRIDGES

APPENDIX A: CROSS FRAME STIFFNESS WITH RESPECT TO DISTORTION-INDUCED FATIGUE

APPENDIX C: INFLUENCE SURFACES RELATING LOAD PLACEMENT AND WEB GAP STRESSES

APPENDIX D: A DETAILED LOOK AT WEB GAP STRESSES

LIST OF FIGURES

PART 1: DISTORTION-INDUCED FATIGUE IN STEEL BRIDGES: CAUSES, PARAMETERS, AND FIXES

PART 2: PARAMETRIC ANALYSIS OF CROSS FRAME CONFIGURATION ON DISTORTION-INDUCED FATIGUE IN SKEWED STEEL BRIDGES

APPENDIX A: CROSS FRAME STIFFNESS WITH RESPECT TO DISTORTION-INDUCED FATIGUE

APPENDIX B: EFFECT OF WEB GAP LENGTH OF FATIGUE SUSCEPTIBILITY

APPENDIX C: INFLUENCE SURFACES RELATING LOAD PLACEMENT AND WEB GAP STRESSES

APPENDIX D: A DETAILED LOOK AT WEB GAP STRESSES

PART 1: DISTORTION-INDUCED FATIGUE IN STEEL BRIDGES: CAUSES, PARAMETERS, AND FIXES

H. L. Hassel[1], A. S. Hartman[2], C. R. Bennett[3], A. B. Matamoros[4], and S. T. Rolfe[5]

ABSTRACT

Distortion-induced fatigue in steel bridges is a continuing problem for bridge engineers. Accordingly, a cumulative review and discussion of scholarly literature on this topic as well as focused analytical research aimed at studying bridge system performance when various retrofit techniques are applied to connection details are described.

Driving forces behind distortion-induced fatigue are presented, including the effects of bridge system geometry and specific detail geometries. Retrofit techniques including positive attachment, back-up transverse stiffeners, slotted connection stiffeners, and removal of lateral brace elements were studied analytically to determine effectiveness. Results from finite element analyses are presented showing relative success of various retrofit techniques. Appropriateness of retrofit techniques under various conditions is also disseminated.

INTRODUCTION

Steel bridges designed prior to the mid-1980s were not always detailed in a manner consistent with current industry standards. Many steel bridges of this era were constructed with cross frames connected to the girder web through transverse connection plates; however, no positive connection was provided between the transverse connection plates and girder flanges. As differential deflection occurred between bridge girders under live loading, lack of connection tended to allow cross frames to pull or push on the girder web, resulting in large cyclic secondary stresses in the weak web gap region. This phenomenon is termed distortion-induced fatigue.

Many of these aging bridges now require regular inspection and repair to address cracking due to distortion-induced fatigue. To adequately understand and effectively retrofit such bridges, it is

University of Kansas, 1530 W. 15th St., Lawrence, KS 66045
[1] Heidi L. Hassel, Graduate Research Assistant, University of Kansas, heidihassel@ku.edu
[2] Amanda S. Hartman, Graduate Research Assistant, University of Kansas, arch-asz@ku.edu
[3] Caroline R. Bennett, PhD, Assistant Professor, University of Kansas, crb@ku.edu
[4] Adolfo B. Matamoros, PhD, Associate Professor, University of Kansas, abm@ku.edu
[5] Stanley T. Rolfe, PhD, A.P. Learned Distinguished Professor, University of Kansas, srolfe@ku.edu

important to examine and compare commonly used retrofit techniques. It is also important to consider the effects retrofits have on the bridge from a system-oriented perspective, rather than considering isolated connections outside of their context. This paper provides an extensive literature review of the causes, parameters, and potential fixes associated with distortion-induced fatigue as well as a finite element study on the effectiveness of common retrofit techniques. The objective of this research was to investigate stress reduction resulting from retrofit techniques and compare the success of each in multiple bridge configurations to identify techniques most suitable for a given bridge geometry.

OBJECTIVE

The objective of this research was to investigate stress reduction resulting from various retrofit techniques and compare the success of each in multiple bridge configurations to identify techniques most suitable for a given bridge geometry.

BACKGROUND

DISTORTION-INDUCED FATIGUE OVERVIEW

Lateral bracing in steel girder bridges stabilizes girders during construction, provides resistance to transverse loading, and helps distribute live loading laterally between girders (Tedesco et al. 1995). During the 1930's several failures occurred in European bridges resulting from welds between connection stiffeners and girder tension flanges (Fisher and Keating 1989). In an effort to prevent fatigue damage, common practice was to provide no positive attachment between connection stiffeners and girder flanges.

Lack of connection creates a weak web gap region susceptible to out-of-plane distortions and fatigue. Uneven loading of girders at equal stations along the bridge induce differential deflections between adjacent girders causing rotation of lateral bracing members. Because the girder top flange is restrained by the deck, out-of-plane displacement is concentrated in the flexible web gap region. Resulting secondary stresses in the web gap can lead to distortion-induced fatigue. Although current AASHTO (2007) specifications require positive attachment between transverse stiffeners and girder flanges, bridges constructed prior to 1980 are at risk of experiencing damaged due to distortion-induced fatigue.

PARAMETERS AFFECTING DISTORTION-INDUCED FATIGUE

It has proven difficult to form conclusions from the body of literature concerning the region of bridges most vulnerable to distortion-induced fatigue. Roddis and Zhao (2001) found that distortion-induced fatigue cracks most frequently occurred in positive bending moment regions where differential girder deflection and out-of-plane bending moments were highest. Conversely, Khalil et al. (1998) observed eight of nine fatigue cracks discovered occurred in the negative moment region in a bridge under investigation. The issue is further complicated by conflicting literature as to whether the web gap region adjacent to the top or bottom girder flange tends to be at greater risk. Fisher et al. (1990) concluded that cracks are most likely to form in web gaps adjacent to the girder top flange unless staggered diaphragms are used.

BRIDGE GEOMETRY

Distortion-induced fatigue is a complicated issue largely influenced by bridge geometry. Skew angle, span length, girder spacing, and deck thickness influence differential deflection between adjacent girders and therefore, affect distortion-induced fatigue. Decreased span length and increased girder spacing both amplify differential deflection, except when the bridge span approaches truck length. As girder length increases and the bridge becomes increasingly flexible, lateral bracing more effectively distributes load between girders, and the bridge displaces vertically with less differential deflection (Berglund and Schultz 2006).

Bridge supports are often skewed to accommodate highway alignments. At equal stations along skewed bridges, each girder is subjected to varied bending moment and deflection under uniform loading. Increasing skew angle increases the bridges differential deflection and susceptibility to distortion-induced fatigue (Berglund and Schultz 2006). Skew angle also influences lateral bracing configuration.

LATERAL BRACING CONFIGURATION

Lateral bracing helps distribute live loads among girders and therefore impacts the resulting differential deflections and web gap stresses in multi-girder steel bridges. There are numerous lateral bracing configurations because brace type and placement can both be varied widely. Use of cross braces instead of bent-plate diaphragms have been shown to significantly reduce

maximum differential deflection (Li and Schultz 2005). Furthermore, K-type truss diaphragms create smaller secondary stresses in web gaps than X-type cross frames (Fisher et al. 1990).

Multiple lateral brace configurations may be used in skewed bridges, including braces placed parallel to the skew angle, perpendicular to the girders' webs, and staggered. Cross frames or diaphragms placed parallel to skew angle and directly across from each other is optimal, but not always practical. Back-to-back bracing members have a balancing effect on out-of plane bending stresses (Barth and Bowman 2001). Placing cross frames parallel to skew angle allows lateral bracing members to be attached to adjacent girders at equal points along the member where girders are subjected to equal bending moments and deflection under uniform loading. At high skew angles, braces placed parallel to skew angle tend to become excessively long and flexible and therefore less effective at distributing load. Current AASHTO (2007) Specifications require that lateral bracing members in bridges with skew angles great than 20 deg. be placed perpendicular to girder webs. In such bridges, lateral bracing can be either non-staggered or staggered. Non-staggered, back-to-back brace placement allows brace forces to utilize the balancing effect, but braces are attached to extremely different points along each girder which increases the differential deflection braces undergo. Therefore, braces are often staggered. Fraser et al. (2000) reported that fatigue cracks were more pronounced in bridges with staggered diaphragms than in bridges with non-staggered diaphragms, but Barth and Bowman (2001) concluded the opposite. This is yet another conflicting conclusion in the literature describing distortion-induced fatigue in steel bridges.

Ongoing research at the University of Texas in Austin involves the use of half-pipe shapes instead of bent-plate transverse connection stiffeners in skewed bridges with cross frames oriented parallel to skew angle is being investigated. Initial results indicate the proposed connection detail stiffens the connection significantly, allowing cross frame spacing to be increased due to higher efficiency of fewer cross frames. A stiffer connection combined with a reduced number of cross frames dramatically decreases bridge susceptibility to distortion-induced fatigue (Quadrato et al. 2009).

LOCAL WEB GAP GEOMETRY

Web gap geometry is thought to influence the amount of secondary stresses induced in the web gap region. According to a survey conducted by Fisher et al. (1990), the web gap length (the

vertical dimension between the inside of the flange and the weld attaching the connection stiffener) typically ranges from 6.35 to 102mm [0.250 to 4.00in]. Web gaps must absorb the out-of-plane displacement. Since smaller web gaps have less space and material to absorb this displacement, the risk of distortion-induced fatigue cracking is increased with decreased web gap length (Fisher et al. 1990).

DISTORTION-INDUCED FATIGUE RETROFIT TECHNIQUES

Out-of-plane distortion or other secondary stresses at fatigue sensitive details are responsible for an estimated 90% of all fatigue cracking in steel bridges (Connor and Fisher 2006). Therefore, repair and retrofit techniques have been developed to enhance fatigue life of steel bridges including stiffening, softening, or removal of connection elements.

STIFFENING OR SOFTENING OUT-OF-PLANE CONNECTION ELEMENTS

Numerous studies have concluded that fatigue performance can be enhanced by either stiffening the web gap or softening the restraint on the connection; although no guidance is provided in literature as to which solution is more appropriate for a given bridge configuration. Fisher et al. (1990) showed that positive attachment reduced secondary stresses in the web gap region by reducing the magnitude of out-of-plane displacement in the girders web. Positive connection can be accomplished using welds, bolts, epoxy, and/or angles. When welding is used, field weld quality is a concern because overhead welding is required. Angles or WT shapes can be attached to the connection plate and flange to reduce stress concentrations. Bolting to the top flange of the girder may be difficult to implement because the concrete deck must be removed; however, Jones et al. (2008) identified a method using stud-welding wherein a bolted angle connection could be made without deck removal. Stiffness of the connection elements used must also be considered as it has been shown to influence effectiveness (Connor and Fisher 2006).

Softening restraint provided by the connection also tends to reduce stresses in the web gap region. Loosening the connection bolts between the stiffener and girder web when a bolted connection is used may reduce both stresses and out-of-plane distortion (Khalil et al. 1998). Another softening technique involves removal of a portion of the transverse stiffener plate, lengthening the web gap. A hole is drilled in the connection plate and a slot is flame cut between the girder web and connection plate.

Removal of Lateral Brace Elements

An additional method of eliminating secondary stresses in web gap regions is to remove lateral brace elements altogether. In composite bridges, interior lateral braces may not be required due to stability provided by the concrete deck. However, lateral bracing may still be needed at supports to transfer lateral loads. Although removal of bracing has been shown to eliminate secondary stresses in web gaps, this technique has been shown to increase differential deflections between adjacent girders by as much as 25% (Tedesco et al. 1995) and bending moments by as much as 15% (Stallings et al. 1999). Therefore, removal may not be advisable unless the bridge under consideration was designed with a high capacity reserve. Another disadvantage of lateral brace removal is that temporary bracing would be required during deck replacement.

Other Improvement Methods

Several methods have been shown to improve fatigue life of welds including shot peening, hammer peening, laser peening, and ultrasonic impact treatment (UIT). These weld treatment methods aim to induce residual compressive stresses at the weld toe resulting in reduced tensile stress ranges experienced at critical details. Additionally, applications of Carbon Fiber Reinforced Polymers (CFRP) to welded details have been shown to improve fatigue life by reducing the stress demand at the weld toe (Kaan et al. 2008).

After a fatigue crack has initiated, growth can be retarded by drilling a hole at the tip of the crack, reducing the stress concentration and increasing the fatigue life. Crack-stop holes can be used in combination with other methods such as cold expansion or pretensioned bolts which introduce residual compressive stresses at the edges of the hole. A combination of retrofits is also practical because space limitations in connection geometry often do not allow for properly sized crack-stop holes and undersized holes must be used.

Modeling Methodology

Studied Parameters

Four commonly used retrofit techniques were implemented in a right (nonskewed) bridge to determine the effects on secondary stresses in the web gap region and other changes induced in retrofitted bridges. Retrofit techniques modeled included positive attachment, back-up stiffeners, slotted connection stiffeners, and interior cross frame removal. Schemes were implemented on a

local and global scale meaning that in "local" models only the most highly stresses regions were retrofitted, whereas all web gap regions were retrofitted in "global" models. The four rows of cross frames producing the highest stresses and treated in local retrofit models were the third and fourth set of cross frames from either end in the positive moment region of the bridge.

Because back-up stiffeners are more often used in skewed bridges with staggered cross bracing members, the effects of this particular retrofit technique were investigated in a 40 deg. skewed bridge with staggered cross frames as well as the right bridge. Three retrofitting schemes were modeled. A partial depth, 305mm [12.0in] stiffener was used on the top flange and bottom flange, and a model with a full depth stiffener fully fixed to both the top and bottom flanges was also used.

BRIDGE DESCRIPTION

The bridge used for analysis was modeled after American Iron and Steel Institute (AISI) Example 2 (1997). The design of this bridge is widely available and has been used in other scholarly research as geometry representative of a typical bridge to illustrate bridge design concepts (Barth et al. 2004). The bridge consists of two 27.4m [90.0ft] continuous spans with four girders spaced at 3.05m [10.0ft]. The cross sections used in the bridge are shown in Fig. 1.

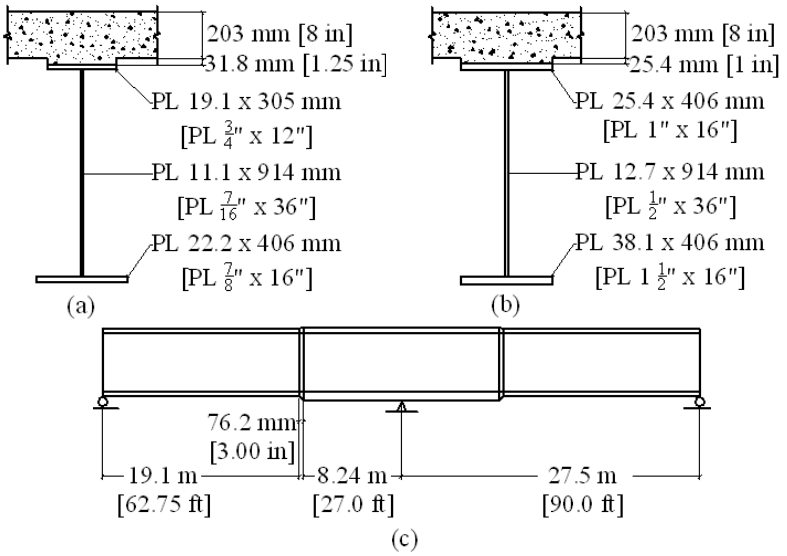

Figure 1. (a) Positive girder cross-section. (b) Negative girder cross-section. (c) Location of positive and negative cross-sections.

X-type cross frames were spaced every 4.58m [15.0ft] along the girders. Fig. 2 shows the plan view of both the right bridge and the skewed bridge. Cross frames were designed based on a

maximum slenderness ratio (KL/r value) of 140 to resist compressive forces since no horizontal loads were applied to the bridge. Equal leg angles, L102x102x15.9mm [L4x4x5/8in] were chosen for brace elements.

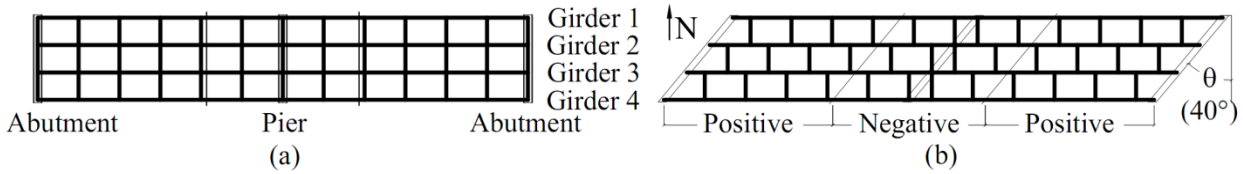

Figure 2. Plan view (a) Right, nonskewed bridge. (b) Skewed, staggered bridge.

FINITE ELEMENT MODELING

Three-dimensional linear-elastic finite element (FE) models were completed using ABAQUS v.6.8-2, commercially available FE software. Each of the four bridge girders were composed of three main parts: bottom flange, web, and top flange with concrete haunch. Other components of the model included cross frames and concrete deck. Various mesh densities were used within the model to develop fine meshes in localized regions with coarse meshes elsewhere. Parts were connected using surface-to-surface tie constraints. Young's moduli were taken as 200GPa [29,000ksi] and 24.9GPa [3605ksi] for steel and concrete, respectively. Poisson's ratio was taken as 0.30 for steel and 0.15 for concrete. Support conditions were applied over a length of 152mm [6.00in] to the bottom flanges of each girder. Pinned conditions were applied to the interior pier while roller conditions were applied at abutments.

Four-node shell elements (S4R) with mesh size of approximately 1.07m [3.50ft] comprised the 203mm [8.00in] thick concrete deck. A pressure of 10.3Pa [0.00015ksi] was applied over a 2.14m [7.00ft] width spanning the entire length of Girder 3. This load was chosen to produce meaningful and noticeable stress responses. Although load placement would be expected to have an effect on distortion-induced fatigue stresses, load was held constant throughout all models to draw valid comparisons between applied retrofits.

Girders, cross frames, and concrete haunches were modeled using eight-node brick elements (C3D8R). Top flanges, bottom flanges, and concrete haunches were meshed at a density of 50.8mm [2.00in]. Girder webs were comprised of various mesh sizes to create very dense meshes in the web gap regions (see Fig. 3). Transitions between structured hexagonal meshes were accomplished through the use of four-node linear tetrahedron elements (C3D4). Mesh

density of the connection stiffeners was also varied to refine output in the web gap region (see Fig. 3).

In order to transition between negative and positive girder dimensions, a 76.2mm [3.00in] region of four-node tetrahedron elements (C3D4) was utilized in the concrete haunch, top flange, web, and bottom flange. Course web mesh size of 50.8mm [2.00in] was applied to the transition regions. This overall modeling strategy was employed to accurately capture system and local response of the bridges studied, while maintaining a reasonable level of computational efficiency needed to accomplish a parametric investigation. Each 3-D bridge model included approximately 750,000 elements and 2.75 million degrees of freedom.

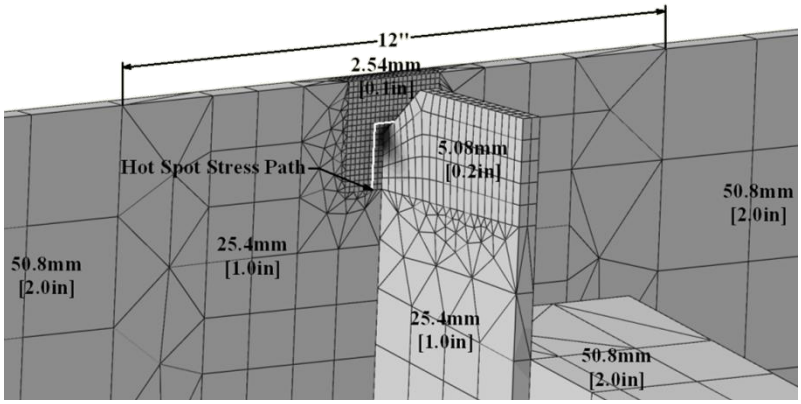

Figure 3. Mesh sizes and Hot Spot Stress path.

RETROFIT TECHNIQUES

Effectiveness of four retrofit techniques in reducing secondary stresses in the web gap regions was investigated. Those studied included positive attachment, back-up transverse stiffeners, slotted connection stiffeners, and interior cross frame removal. The no-retrofit configuration and the first three of these retrofits are shown in Fig. 4.

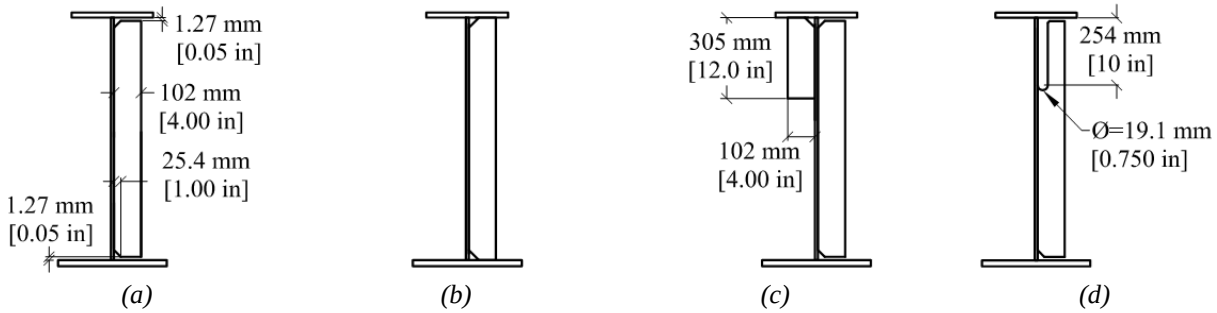

Figure 4. (a) No-retrofit stiffener. (b) Positively attached stiffener. (c) Back-up transverse stiffener. (d) Slotted connection stiffener.

Positive attachment was accomplished by removing the 1.27mm [0.0500in] gaps between the stiffener and flanges and using surface-to-surface tie constraints between the transverse stiffener and both top and bottom flanges. The back-up stiffener was modeled with the same thickness and width as the transverse stiffener plate, but the length was varied. Surface to surface ties were used to connect the back-up stiffener to both the web and adjacent girder flange(s), depending on the configuration used. Back-up stiffeners were meshed identically to no-retrofit connection stiffeners.

Slot dimensions were chosen based on space limitations and suggestions found in the literature surveyed (Fisher et al. 1990 and Fisher and Keating 1989). A slot length of 254mm [10in] was sized to be 20 times the largest web thickness. The hole diameter at the end of the slot was limited to 19.1mm [0.750in] by geometric constraints in the stiffener plate. In practice, the hole should be sized to facilitate a smooth surface so that new areas of stress concentration are not created (Zhao and Roddis 2007). The densely meshed region in both the stiffener and web were extended beyond the slot by 50.8mm [2.00in] so that detailed results could be viewed in the lengthened web gap region.

HOT SPOT STRESS ANALYSIS

Hot Spot Stress (HSS) analysis was utilized to compare stresses induced in bridge web gaps. HSS was chosen over absolute maximum stress because it is less mesh dependant and has been shown to be more reliable in regions of complex geometry. Because the web gap region experiences a complex three-dimensional stress field, maximum principal stress was deemed optimal for comparing stresses in this study. Numerous HSS techniques have been developed, however a simple one point extraction procedure was used herein. The procedure involved determining stress values a set distance from the weld toe and comparing them directly. Stress values were collected a distance of approximately half of the web thickness, 5.08mm (0.200in), from the weld toe on all three sides of each transverse stiffener in the densely meshed region of the girder web as shown in Fig. 3.

RESULTS

All four retrofit techniques studied reduced the web gap stress at applied locations. However, the extent to which each retrofit extended the bridge's fatigue life varied significantly. Table 1

presents the maximum principal web gap stress in each of the right bridge models determined using Hot Spot Stress analysis as well as the percentage change from the no-retrofit model. Location of maximum principal HSS in the right bridge model with no retrofit was observed to be in the top web gap of Girder 4 in the positive moment regions (Fig. 2). Second most highly stressed region was the top web gap of Girder 2 in the positive moment regions.

Table 1. Maximum web gap stresses determined using Hot Spot Stress analysis, right bridge.

	Locally Applied Retrofit		**Globally Applied Retrofit**	
Retrofit Description	***Stress MPa [ksi]***	***% Change from no-retrofit model***	***Stress MPa [ksi]***	***% Change from no-retrofit model***
No Retrofit	103 [14.9]			
Positive Attachment	80.7 [11.7]	-21%	52.5 [7.62]	-49%
Back-Up Stiffener	102 [14.8]	-1%	99.4 [14.4]	-3%
Slotted Stiffener	86.0 [12.5]	-16%	69.2 [10.1]	-33%
Cross Frame Removal	98.5 [14.3]	-4%	45.4 [6.58]	-56%

Vertical girder deflection at each cross frame was also extracted from the analytical models and differential deflection between adjacent girders at every cross frame location (or location of cross frame removal) was computed. The differential deflection between Girders 3 and 4 was deemed most critical due to the location of maximum principal stress in the bridge, although this was not found to be the location of highest differential deflection, Δ. Results and percent change from the no-retrofit model are shown in Table 2.

Table 2. Maximum differential deflection between Girder 3 and 4, right bridge.

	Locally Applied Retrofit		**Globally Applied Retrofit**	
Retrofit Description	***Δ mm [10^{-3} in]***	***% Change from no-retrofit model***	***Δ mm [10^{-3} in]***	***% Change from no-retrofit model***
No Retrofit	0.249 [9.82]			
Positive Attachment	0.222 [8.74]	-11%	0.169 [6.66]	-32%
Back-Up Stiffener	0.408 [9.16]	-5%	0.570 [8.07]	-18%
Slotted Stiffener	0.233 [16.1]	64%	0.205 [22.5]	129%
Cross Frame Removal	0.532 [21.0]	114%	0.773 [30.4]	210%

LOCAL VS. GLOBAL RETROFIT TECHNIQUES

All retrofits were more successful at reducing the maximum web gap stress in the bridge when applied globally rather than locally. Globally-applied retrofits reduced the magnitude of stress demand by more than twice as much as local retrofits. Localized retrofit techniques reduced the stress where the retrofit was applied, but stresses in untreated areas of the bridge remained potentially problematic. In models with slotted stiffeners and removed cross frames stresses in untreated areas actually increased, although maximum stress in the entire bridge decreased. Maximum principal stress at each cross frame location in the top web gap of Girder 4 in models

with the local retrofit are shown in Fig 5. These findings emphasize the importance of treating distortion-induced fatigue on a system (global) level rather than focusing on localized regions in the bridge. Though local retrofitting may theoretically be a cost-saving approach, it was not found to be practical due to disagreement in the literature concerning the location of maximum stresses in bridges, as well as the possibility of transferring distortion-induced fatigue risk to other connections.

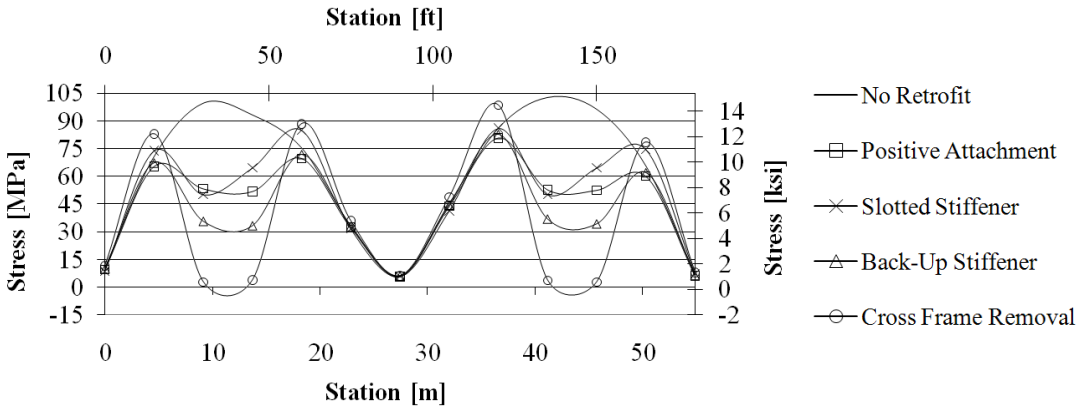

Figure 5. Maximum principal Hot Spot Stress in the top web gap of Girder 4 at each cross frame location in models with the local retrofit.

POSITIVE ATTACHMENT

Positively attaching the transverse stiffener to both the top and bottom flange reduced stresses in the web gap region, thereby extending fatigue life of the connection detail. It decreased both differential deflection and Hot Spot Stress in the bridge. Of the four retrofitting schemes analyzed, it reduced differential deflection the most and produced the second highest reduction in stress. Connections made between the transverse stiffener plates and girder flanges are not expected to be completely rigid in practice, which may decrease the effectiveness of this retrofit technique from that found in the FE models.

BACK-UP STIFFENER

The back-up stiffener was not found to be an effective retrofit when applied to a right, nonskewed bridge. Although it decreased web gap stresses generated in the exterior girders where applied, the stress in Girder 2 increased. Therefore the overall maximum principal stress in the bridge did not decrease significantly.

The no-retrofit, skewed staggered model produced the highest Hot Spot Stresses in the bottom web gaps of the loaded girder in the positive moment regions. Though the location of maximum

stress was different than in the right bridge, results were consistent with those of Fisher et al. (1990). Data for HSS in the web gap region and differential deflection between Girder 3 and 4 are shown in Table 3. Results for a locally retrofitted bridge were consistent with those determined using a right bridge.

Table 3. Maximum prinicpal Hot Spot Stress and differential deflection between Girder 3 and 4 for skewed, staggered bridge with global retrofit.

Retrofit	Stress MPa [ksi]	*% Change from no-retrofit model*	Δ mm [10^{-3} in]	*% Change from no-retrofit model*
No Retrofit	100 [14.6]		1.06 [41.8]	
Top Partial Stiffener	103 [15.0]	3%	0.954 [37.6]	-10%
Bottom Partial Stiffener	51.2 [7.43]	-49%	1.02 [40.0]	-4%
Full Depth Stiffener	35.9 [5.20]	-64%	0.896 [35.3]	-16%

The top partial stiffener was not effective in reducing stress in the bridge because it was not applied at locations of maximum stress. Both the bottom partial stiffener and the full depth stiffener significantly reduced the maximum principal stress in the bridge by almost 50%. All three retrofit schemes reduced differential deflection.

SLOTTED TRANSVERSE STIFFENER

Removal of a portion of the transverse stiffener significantly increased differential deflection as much as 129% in some areas but reduced the maximum principal stress in the bridge, illustrating that differential deflection alone cannot necessarily predict the bridge's susceptibility to distortion-induced fatigue. Literature reviewed noted increased out-of-plane displacement resulting from utilization of the slot retrofit technique as much as four times the original value (Zhao and Roddis 2007). Therefore, the maximum out-of-plane displacement along the path used for HSS analysis was determined at each cross frame location. Out-of-plane displacement increased significantly and magnitudes in retrofitted models were as much as five times larger than in the model with no retrofit. Though out-of-plane displacement increased, the magnitude remained small (under 0.762 mm [0.0300 in]) and therefore, was not regarded as detrimental for this structure.

CROSS FRAME REMOVAL

Complete removal of interior cross frames eliminated the web gap region and associated stress concentrations, reducing the maximum principal HSS in the bridge by 56%. In this study, cross frame removal was most effective at reducing stresses at the original cross frame locations, but

may not be suitable for all bridges. Because interior cross frames were no longer present to help distribute traffic loading among adjacent girders, the differential deflection increased by as much as 210% at some locations. Though the increase was large, it was not considered problematic because the maximum girder deflection increased by less than 0.500mm [0.0200in].

CONCLUSIONS

A thorough review of existing literature concerning the causes of distortion-induced fatigue, parameters which influence a bridge's susceptibility to secondary stresses generated in the web gap regions, and retrofits that can extend the remaining fatigue life of the bridge is presented. A finite-element analysis involving four retrofits including positive attachments, back-up transverse stiffeners, slotted connection stiffeners, and cross frame removal was conducted. Conclusions of this study can be summarized as follows:

- Generally speaking, retrofit techniques should be applied on a global basis. Retrofitting every connection in the bridge reduced the maximum stress more than twice as much as only treating the most highly stressed regions.
- Connection stiffening techniques reduced the amount of differential deflection between adjacent girders, but connection softening techniques and cross frame removal increased differential deflection.
- Positive attachment reduced differential deflection by the greatest amount and reduced the maximum principal stress in the bridge by almost 50%.
- Back-up stiffeners were found to not be suitable for right, nonskewed bridges, but were extremely effective in skewed, staggered bridges. Globally applied back-up stiffeners were found to reduced the maximum stress in the bridge (originally found in the positive moment regions) most when either partial depth and attached to the bottom web gap region or full depth were used.
- Partial removal of the transverse stiffener through use of a slot technique reduced the stress concentrations in the web gap region by over 30%.
- Cross frame removal reduced secondary stresses in the web gap regions over 55% and was the most effective of the retrofits studied, although removal may not be a practical solution for all bridges.

Many bridges are susceptible to distortion-induced fatigue and identification of effective retrofits is essential to extending useful life. Finite element analysis performed demonstrates the importance of considering the bridge as a system rather than individual connections in an isolated sense (global vs. local), when evaluating performance of retrofit techniques. Bridge parameters not only affect the bridges' fatigue risk, but success of repair and retrofit schemes. This study highlighted the importance of quantifying stresses in the bridge rather than using differential deflection alone to predict fatigue risk. Findings of this analysis are intended to help further guide bridge engineers in selecting and implementing retrofits in steel girder bridges.

ACKNOWLEDGEMENTS

The authors are grateful for support from the Kansas Department of Transportation (KDOT) and the University of Kansas Transportation Research Institute (KU TRI). The authors would also like to gratefully acknowledge support provided through Pooled Fund Study TPF-5(189), which includes the following participating State DOTs: Kansas, California, Iowa, Illinois, New Jersey, New York, Oregon, Pennsylvania, Tennessee, Wisconsin, and Wyoming, as well as the Federal Highway Administration.

REFERENCES

American Iron and Steel Institute (AISI) Example 2: Two-Span Continuous Composite I Girder (1997). *American Iron and Steel Institute*.

American Association of State Highway and Transportation Officials (AASHTO). (2007). *Standard Specifications for Highway Bridges*, Washington, D.C.

Barth (Grider), A.S. and Bowman, M.D. (2001). "Fatigue Behavior of Welded Diaphragm-to-Beam Connections." *Journal of Structural Engineering*, 127(10), 1145-1152.

Barth, K.E., Hartnagel, B.A., White, D.W., and Barker, M.G. (2004). "Recommended Procedures for Simplified Inelastic Design of Steel I-Girder Bridges." *Journal of Bridge Engineering*, 9(3), 230-242.

Berglund, E. and Schultz, A. (2006). "Girder Differential Deflection and Distortion-Induced Fatigue in Skewed Steel Bridges." *Journal of Bridge Engineering*, 11(2), 169-177.

Connor, R. J. and Fisher, J. W. (2006). "Identifying Effective and Ineffective Retrofits for Distortion Fatigue Cracking in Steel Bridges Using Field Instrumentation." *Journal of Bridge Engineering*, 11(6), 745-752.

Fisher, J. W., Jian, J., Wagner, D. C., and Yen, B. T. (1990). "Distortion-Induced Fatigue Cracking in Steel Bridges." *National Cooperative Highway Research Program Report #336,* Transportation Research Board, National Research Council, Washington, D. C.

Fisher, J.W. and Keating, P.B. (1989). "Distortion-Induced Fatigue Cracking of Bridge Details with Web Gaps." *Journal of Constructional Steel Research,* 12(3-4), 215-228.

Fraser, R.E.K., Grondin, G.Y., and Kulak, G.L. (2000). "Behavior of Distortion-Induced Fatigue Cracks in Bridge Girders." *Structural Engineering Report No. 235*.

Jones, J., Bennett, C., Matamoros, A., Rolfe, S., and Roddis, K. (2008). "Fighting fatigue in steel bridges," TR News, Transportation Research Board (TRB), Nov/Dec, Issue 259.

Kaan, B., Barrett, R., Bennett, C., Matamoros, A., and Rolfe, S. (2008). "Fatigue Enhancement of Welded Coverplates Using Carbon-Fiber Composites." Proc. of the 2008 ASCE/SEI Structures Congress, Vancouver, ABC, April 24-26, 2008.

Khalil, A., Wipf, T. J., Greimann, L, Wood, D. L, and Brakke, B. (1998). "Retrofit Solution for Out-of-Plane Distortion of X-Type Diaphragms Bridges." *Transportation Conference Proceedings, Iowa Department of Transportation*, 99-102.

Li, H. and Schultz, A. E. (2005). "Analysis of Girder Differential Deflection and Web Gap Stress for Rapid Assessment of Distortional Fatigue in Multi-Girder Steel Bridges." *Final Report 2005-38,* Minnesota Department of Transportation, St. Paul, MN.

Quadrato, C., Battistini, A., Helwig, T., Engelhardt, M., and Frank, K. "Effect of Cross Frame Connection Details on Stability of Steel Bridges with Skewed Supports." University of Texas, Austin. http://www.aisc.org/assets/0/1209478/1209480/1271820/39248d5d-83ad-4575-ae4c-4672c2486359.pdf [accessed 12/16/2009].

Roddis, W.M.K. and Zhao, Y. (2001). "Out-of-Plane Fatigue Cracking in Welded Steel Bridges: Why It Happened and How It Can Be Repaired." Welding Innovation, 27(2), 2-7.

Stallings, J. M., Cousins, T. E., and Stafford, T. E. (1999). "Removal of Diaphragms from Three-span Steel Girder Bridges." Journal of Bridge Engineering, 4(1), 63-70.

Tedesco, J.W.; Stallings, J. M.; and Tow, D.R. (1995). "Finite Element Method Analysis of Bridge Girder-Diaphragm Interaction." Computers and Structures, 56(2-3), 461-473.

Zhao, Y. and Roddis, W. M. K. (2007). "Fatigue Behavior and Retrofit Investigation of Distortion-Induced Web Gap Cracking." *Journal of Bridge Engineering*, 12(6), 737-745.

PART 2: PARAMETRIC ANALYSIS OF CROSS FRAME CONFIGURATION ON DISTORTION-INDUCED FATIGUE IN SKEWED STEEL BRIDGES

ABSTRACT

A parametric analysis was conducted to investigate the effects of skew angle, cross frame spacing, and bracing configuration on distortion-induced fatigue as quantified by hot spot stress in the web gap region, as distortion-induced fatigue cracking remains problematic in existing multi-girder steel bridges throughout the country. Three bracing configurations were evaluated, including bridges with cross frames place parallel to skew angle and perpendicular to the girder line, both staggered and unstaggered. Bridges with skew angles ranging from 0 to 50 deg. and cross frame spacing ranging from 2.29 to 9.14 m [7.50 to 30.0 ft] were included in this study. In addition, an influence surface analysis was conducted on three bridge variations to better understand the relationship between load placement, location of maximum web gap stress, and web gap stress magnitude. Cross frame stiffness was also investigated and shown to be an important parameter that significantly impacts bridge susceptibility to distortion-induced fatigue. Results of finite element analyses are presented showing relative web gap stress magnitudes and locations within each bridge arrangement most vulnerable to distortion-induced fatigue.

1: INTRODUCTION

1.1: PROBLEM STATEMENT

Many multi-girder steel bridges designed prior to the mid-1980's contain fatigue prone connection details that have resulted in localized cracking and high susceptibility to distortion-induced fatigue. Cross frames and diaphragms span between girders to brace steel girders during construction and help distribute live loads after the deck is in place. As adjacent girders deflect differing amounts from uneven traffic loading, cross frames or diaphragms rotate causing out-of-plane distortion and high cyclic stresses at the intersection of the web and transverse connection stiffeners. This mechanism is known as distortion-induced fatigue. Stress concentrations and cracking occur in a weak region of the web, known as the web gap. The web gap was created due to common detailing practice in which the transverse stiffener was cut short of and not connected to the adjacent flange, creating a short, highly flexible region on the web.

Approximately 90% of fatigue cracking occurs due to secondary stresses at fatigue-sensitive details (Connor and Fisher 2006). Therefore, it is critical to evaluate parameters which influence vulnerability in order to identify highly susceptible bridges and implement effective repair and retrofit techniques. It is also important to understand distortion-induced fatigue to ensure repair methods will not create additional problems in the future.

1.2: OBJECTIVE

The objectives of this analysis were to quantify the effects of skew angle, cross frame spacing, bracing configuration, and cross frame stiffness on distortion-induced fatigue using web gap stresses, to identify regions within bridges where cracking is most likely to occur, and to evaluate the relationship between load placement and web gap stresses. Detailed finite element models were used to investigate these parameters and gain a better understanding of distortion-induced fatigue to help extend the fatigue life of vulnerable bridges.

2: BACKGROUND

2.1: BRIDGE GEOMETRY

Distortion-induced fatigue is especially problematic in bridges with skewed supports, designed to accommodate highway alignment. Differential deflection is magnified in skewed bridges as adjacent girders at equal stations along the bridge are at different span points and deflect differing amounts even under uniform loading (Berglund and Schultz 2006). As a result, bridges with large skew angles are more susceptibility to distortion-induced fatigue cracking (Fisher and Mertz 1984).

Three primary bracing configurations are used in skewed bridges and are shown in Figure 1. For the purposes of this paper, the term cross frame will be used to denote truss type connections, diaphragm will be used to describe connection made through a larger, single member, and bracing will be used to denote instances in which either may be used. Bracing may be placed parallel to the skew angle or perpendicular to the girder line in a staggered or unstaggered configuration. These configurations will be referred to as skewed-parallel, skewed-staggered, and skewed-unstaggered throughout this paper. Skewed-parallel configurations are generally considered least susceptible to distortion-induced fatigue, as both ends are attached at the same point along adjacent girders. The American Association of State Highway and Transportation

Officials (AASHTO 2007) requires bracing be placed perpendicular to the girder line in bridges with skew angles larger than 20 deg. due to increased length and flexibility and presumed ineffectiveness at distributing loads. However, design provisions in some states allow the use of skewed-parallel configuration beyond this limit to reduce potential differential deflection and associated distortion-induced fatigue vulnerability (KDOT 2010).

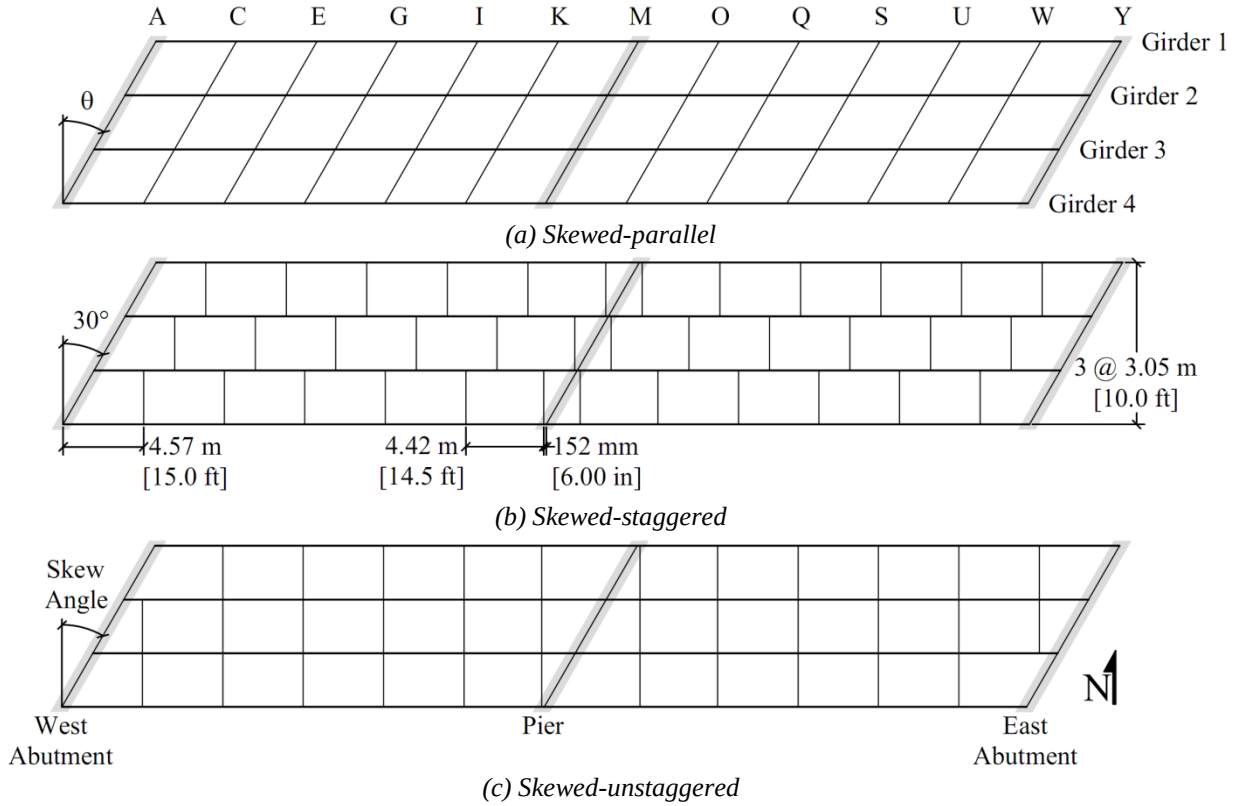

Figure 1: Bridge configurations (30 deg. skew with 4.57 m [15.0 ft] cross frame spacing)

For bridges with bracing placed perpendicular to the girder line, previous research is not clear on which configuration performs better with respect to distortion-induced fatigue. Many studies observed large, out-of-plane girder movements in bridges with skewed-staggered bracing, making them less effective at transferring gravity loads laterally (Fraser et al. 2000, Barth and Bowman 2001, and Hartman et al. 2010). Lab testing of both configurations showed cracks were more common in the unstaggered configuration, because back-to-back diaphragms were more rigid, acting as one continuous member (Barth and Bowman 2001). Therefore, cracking may be less likely in skewed-staggered bridges due to reduced load transfer, but this is not necessarily a desirable characteristic. After cracks occurred, out-of-plane movement in skewed-staggered

bridges magnified the effects of distortion-induced fatigue and further reduced the ability of the bracing to transfer loads (Fraser et al. 2000; Barth and Bowman 2001).

Other geometric parameters which have been shown to impact bridge susceptibility to distortion-induced fatigue include girder spacing, span length, local web gap geometry, and bracing type (Berglund and Schultz 2006, Castiglioni et al. 1988, Fisher and Mertz 1984, and Fisher et al. 1990)

2.2: Stiffness of Cross Frames and Diaphragms

Bracing stiffness has not been sufficiently evaluated as a parameter associated with distortion-induced fatigue, although it controls the ability of each brace to attract and distribute load. No previous research was found that directly investigated impacts of bracing stiffness on distortion-induced fatigue, although some studies have considered similar parameters (Fisher et al. 1980; Li and Schultz 2005). Stiffness of bracing and connecting elements is an essential issue, especially for heavily skewed bridges. Stiffness can be significantly reduced when bracing is not placed perpendicular to the girder line. In addition to a reduction for increased length, bracing element stiffness (β_{br}) is multiplied by a $cos^2\theta$ term to determine the stiffness of skewed bracing $\beta_{br,skew}=\beta_{br}cos^2\theta$, making brace stiffness a function of $cos^3\theta$ (Wang and Helwig 2008). Research has also shown that bracing stiffness (β_b) is dependent on stiffness of both the brace element and connection stiffener (β_{conn}) (Yura et al. 1992; Yura 2001). This relationship can be described using the expression $1/\beta_b = 1/\beta_{br} + 1/\beta_{conn}$ (AISC 2005).

2.3: Location of Maximum Stress

The location within a bridge most vulnerable to distortion-induced fatigue cracking is unclear from previous research. This is likely due to the large variety of bridge geometry and influence of previously described parameters. Studies by Zhao and Roddis (2001; 2003) found cracks in regions of positive bending of continuous-span girders. Other researchers noted cracking in regions of negative bending (Jajich and Schultz 2003; Khalil et al. 1998).

Cracks have been noted in web gaps adjacent to both the top and bottom girder flanges. Bridge configuration may impact the location of cracking, as Fisher et al. (1990) noted that cracks occurred only in top web gaps unless staggered diaphragms were used. Within each web gap

there are several possible points of crack initiation. Both the flange to stiffener and flange to web weld are susceptible to distortion-induced fatigue. Because the flange to web weld is typically smooth and of better quality, it can reasonably be expected to have a higher fatigue resistance. Although the stress range may be lower at the flange to stiffener weld, cracking most frequently occurs here (Fisher et al. 1990).

3: MODELING METHODOLOGY

3.1: PARAMETERS CONSIDERED

Distortion-induced fatigue has caused cracking in many steel, multi-girder highway bridges. Geometric characteristics such as skew angle and bracing configuration widely vary and have a significant impact on bridge susceptibility to distortion-induced fatigue. Accordingly, four parameters were investigated to determine their effects on distortion-induced fatigue as quantified by web gap stress: bridge skew angle, cross frame spacing, bracing configuration, and cross frame stiffness.

Table 1 shows a matrix of the 60 bridge variations considered. Bracing configurations are illustrated in Figure 1 for the 30 deg. skewed bridge with 4.57 m [15.0 ft] cross frame spacing. The skewed-parallel bridge configuration was only modeled for skew angles up to 40 deg. to realistically capture use by state DOTs, although AASHTO (2007) limits its use to bridges with a 20 deg. maximum skew angle (KDOT 2010).

Table 1: Parameters considered

Skew Angle	*Cross Frame Spacing, m [ft]*			
	2.29 [7.50]	*4.57 [15.0]*	*6.86 [22.5]*	*9.14 [30.0]*
0	N*	N	N	N
10	P S U	P S U	P S U	P S U
20	P S U	P S U	P S U	P S U
30	P S U	P S U	P S U	P S U
40	P S U	P S U	P S U	P S U
50	S U	S U	S U	S U

*N = Non-skewed, P = skewed-Parallel, S=skewed-Staggered, and U=skewed-Unstaggered

Each bridge configuration was loaded using the AASHTO (2007) fatigue truck, placed to induce maximum web gap stress. Influence surfaces for web gap stresses were used to determine truck

placement. Results of the influence surface analysis and details regarding load placement are described in Section 4: Loading on Bridge Deck.

3.2: BRIDGE GEOMETRY

3.2.1: OVERALL DIMENSIONS

Bridge geometry was adapted from American Iron and Steel Institute (AISI), Design Example 2 (1997), as design is well understood and widely available. Geometry can be considered not atypical of a multi-girder highway overpass, and has been used in other scholarly literature to demonstrate different bridge engineering concepts (Barth et al. 2004). The bridge has two 27.4 m [90.0 ft] spans, composed of four continuous girders spaced at 3.05 m [10.0 ft] as presented in Figure 1. Girders were composite, topped by a 203 mm [8.00 in] thick concrete deck with a 1.07 m [3.50 ft] overhang on each side, totaling 11.3 m [37.0 ft] in width. Separate built-up cross sections were used in regions of positive and negative bending. Each girder was supported by a pin at the central pier and roller supports at both ends. Dimensions are shown in Figure 2.

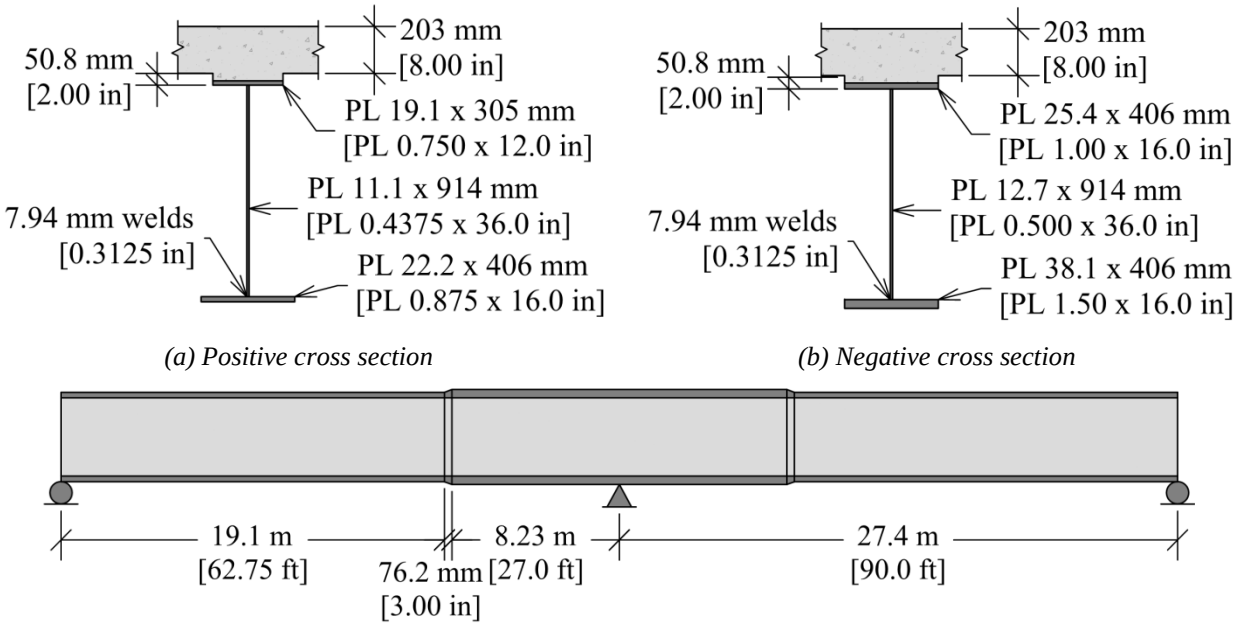

(a) Positive cross section *(b) Negative cross section*

(c) Overview of girder

Figure 2: Bridge geometry

3.2.2: CROSS FRAMES

X-type cross frames were used in all bridge configurations studied and consisted of three equal leg angle sections spanning between connection stiffeners as shown in Figure 3. In bridges with skewed-parallel configurations, cross frame length increased with skew angle. In this situation,

bent plate stiffeners were used to capture realistic construction considerations, making both cross frame element and connection stiffness important parameters. A secondary study was conducted to ensure cross frame element/connection stiffener (angle/stiffener) combinations were selected to have approximately constant stiffness, so the effects of cross frame spacing, skew angle, and bracing configuration could be clearly evaluated in addition to the effect of cross frame stiffness on distortion-induced fatigue.

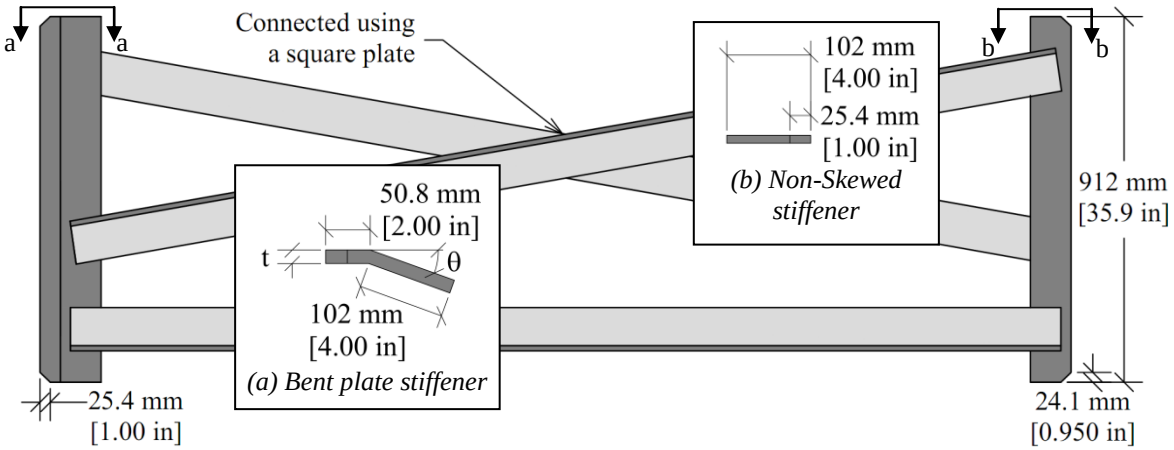

Figure 3: Connection stiffener geometry

Equal leg angles for skewed bridges were chosen based on both slenderness ratio and cross frame stiffness. Equal leg angle sizes not included in the American Institute of Steel Construction's Steel Construction Manual (AISC Manual 2005) were considered due to high sensitivity of stiffness parameters and need to match cross frame stiffness as closely as possible. An L108x108x12.7 mm [L4.25x4.25x0.500 in] angle was selected for the non-skewed bridge based on maximum slenderness ratio of 140 (AASHTO 2007). Slenderness ratio for single angles was computed using provisions in AISC, Section E5 (2005). Cross frame stiffness was compared based the approximate relative stiffness, $A\cos^3\theta$ where A is the cross-sectional area of one angle (mm^2 [in^2]) and θ is the skew angle (deg.) (Yura 2001; Wang and Helwig 2008). Accordingly, angles were selected to have a slenderness ratio less than 140 and an $A\cos^3\theta$ term closest to that of the non-skewed bridge.

Flexibility of bent plate stiffeners and its effect on cross frame stiffness is a very complex problem. Therefore, sub-models were created and analyzed to determine the stiffener thickness for each skew angle that would result in cross frame forces similar to those produced in the non-

skewed configuration. Sub-models consisted of three 9.14 m [30.0 ft] long sections of girder connected by cross frames spaced every 4.57 m [15.0 ft]. A concentrated load was applied to the center girder at mid-span. Sub-models with varied skew angle and bent plate stiffener thickness were evaluated and lateral forces developed in cross frame members at mid-span were used match cross frame stiffness in skewed sub-models to the non-skewed sub-model and select the appropriate stiffener thickness. Stiffener thickness required for bridges with 40 and 50 deg. skew angles using the above outlined procedure was over 38.1 mm [1.50 in]. This was considered unrealistic. Therefore, a larger equal leg angle was selected for the cross frame elements, so a maximum stiffener thickness of 25.4 mm [1.00 in] would be sufficient to match lateral forces produced in the non-skewed sub-model. Skewed cross frames in 50 deg. skewed bridges used the same angle/stiffener combination as 40 deg. skewed bridges, thus did not have equal cross frame stiffness due to extremely large angle/stiffener requirements. It should be noted that while it is recognized that a 25.4 mm [1.00 in] thick stiffener thickness is also not realistic, the authors found the stiffener properties drive behavior in bridges with large skew angles. Angle sizes and connection stiffener thickness for each skew angle are given in Table 2. Detailed results from sub-modeling can be found in Appendix A: Cross Frame Stiffness with respect to Distortion-Induced Fatigue. Variation of web gap length was also evaluated before 25.4 mm [1.00 in] was chosen and results are presented in Appendix B: Effect of Web Gap Length on Fatigue Susceptibility.

Table 2: Cross frame dimensions

Skew, deg.	*Angle, mm [in]*	*Connection Stiffener Thickness, mm [in]*
0	L108x108x12.7 [L4.25x4.25x0.500]	9.53 [0.375]
10	L114x114x12.7 [L4.50x4.50x0.500]	9.53 [0.375]
20	L121x121x19.1 [L4.75x4.75x0.500]	19.1 [0.750]
30	L133x133x19.1 [L5.25x5.25x0.750]	22.2 [0.875]
40	L152x152x25.4 [L7.00x7.00x1.00]	25.4 [1.00]
50	L152x152x25.4 [L7.00x7.00x1.00]	25.4 [1.00]

3.3: Finite Element Modeling

Detailed three-dimensional Finite Element (FE) models of the entire bridge superstructure were created using Abaqus v.6.8-2 for parametric analysis (Simulia 2008). The linear-elastic models contained highly refined meshing in web gap regions and less dense mesh away from the area of interest. C3D8R brick elements were used for the majority of the model, but C3D4 tetrahedral and C3D6 wedge elements were used to transition between mesh sizes. On average, models contained approximately 4 million elements and 27 million degrees of freedom.

The concrete deck was modeled with a modulus of elasticity of 24,850 MPa [3,605 ksi] and Poison's ratio of 0.150. A sensitivity analysis was performed to select a 152 mm [6.00 in] mesh size for the bridge deck, making the deck two elements thick. Skewed bridge decks contained wedge elements near bridge ends. Girders were composed of steel with a modulus of elasticity of 200,000 MPa [29,000 ksi] and Poison's ratio of 0.300. A maximum mesh size of 50.8 mm [2.00 in] was used for all steel parts. Mesh sizes near the web gap region are shown in Figure 4. A 76.2 mm [3.00 in] wide region was used to transition between girder cross sections instead of modeling splices.

Surface-to-surface ties were used to attach parts. Welds (paired with ties) were used to connect the flanges, webs, and cross frames. A mesh size of 3.97 mm [0.156 in] was used for welds to maintain a reasonable aspect ratio and welds were modeled with the same material properties as other steel parts. Boundary conditions were achieved by applying translational restraint over a narrow, 50.8 mm [2.00 in] strip of the bottom flanges. Interactions between the connection stiffeners and girder flanges were defined using hard contact, which caused the connection stiffeners to bear on girder flanges when rotation was significant.

3.4: Hot Spot Stress Analysis

Hot Spot Stresses (HSSs) were used to quantify and compare bridge susceptibility to distortion-induced fatigue. HSS was chosen as the basis for comparison because it is more reliable in regions of complex mesh and less mesh-dependant than maximum nominal stress magnitude. Though many procedures are available, a simple one point procedure was used in which stress approximately 5.08 mm [0.200 in] away from the weld toe (about half the web thickness) was extracted and used to represent the stress concentration at the connection. Maximum tensile

principal HSS was used to compare stress magnitudes because distortion-induced fatigue results from stress in all three directions.

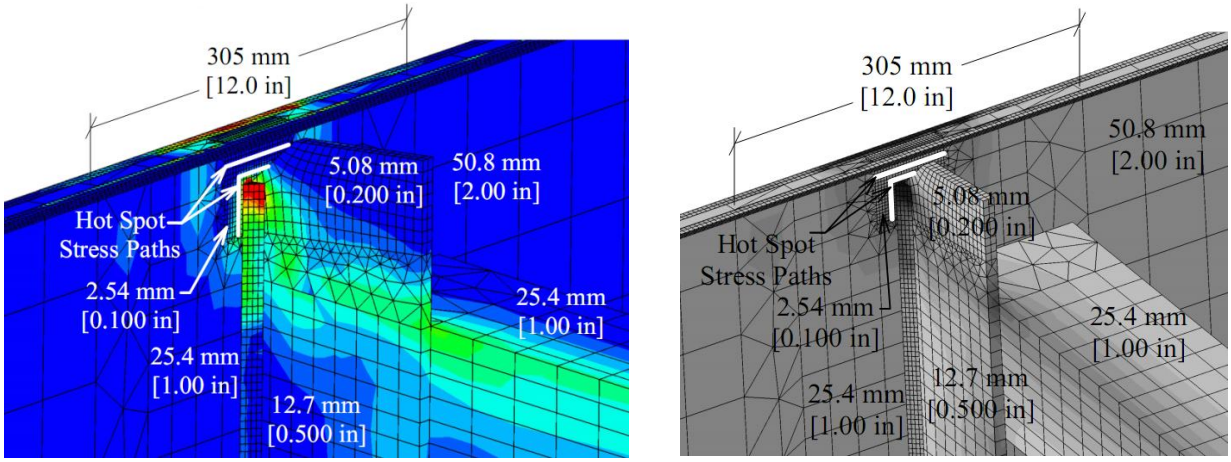

Figure 4: Hot spot stress analysis and mesh sizes

Two separate regions of high stress concentration were investigated as suggested in Fisher et al. (1990). Hot Spot Stress 1 (HSS#1) and Hot Spot Stress 2 (HSS#2) will be used to denote the stress concentration in the web near the cross frame to web weld and flange to web weld respectively. Stress magnitudes along each path were determined and the maximum along each was taken as representative of the connection. Stress paths are shown in Figure 4 and magnitudes were noted on both sides of the web even when cross frames were not placed back-to-back. HSS#1 was considered separately from HSS#2 because the importance of each may be heavily based on the individual bridge geometry and weld quality. Directional stresses (x, y, and z) were compared for both types of stress concentrations and the primary directional contributors are described in Appendix D: A Detailed Look at Web Gap Stresses.

4: Loading on Bridge Deck

4.1: Overview

AASHTO (2007) fatigue loading requires investigation of a fatigue truck placed anywhere on the bridge to cause maximum demand. Truck placement to induce maximum HSS was unclear, as previous studies have concentrated on placing load to maximize differential deflection (Berglund and Schultz 2006). HSS in the web gap region may provide a more accurate comparative measure, because fatigue and fracture are driven by cyclic stresses. However, prior research has demonstrated that the location of maximum differential deflection does not always correspond to

the location of maximum hot spot stress (Hartman et al. 2010). Therefore, three influence surfaces, each based on more than 250 three-dimensional FEMs similar in level of detail as those used in the parametric study, were developed to establish a more clear relationship between load placement, HSS magnitude, and location of maximum web gap stress. An overview of the study conducted is presented here, but additional details can be found in Appendix C: Influence Surfaces Relating Load Placement and Web Gap Stresses. The impact factor (*IM = 1.15*) and load factor ($\gamma = 0.75$) for the fatigue load case result in a reduction of the unfactored fatigue truck loading (AASHTO 2007). Therefore, only the unfactored fatigue truck loading was used.

4.2: MODELING METHODOLOGY: INFLUENCE SURFACES

A non-skewed, 40 deg. skewed-parallel, and 40 deg. skewed-staggered bridge were investigated with bridge geometry and modeling techniques as described in Section 3 with cross frames spaced 4.57 m [15.0 ft] apart. Influence surface analysis was conducted before cross frame geometry refinement for stiffness was completed. Cross frames placed parallel to skew in skewed-staggered and skewed-parallel bridge configurations consisted of L152x152x25.4 mm [L6.00x6.00x1.00 in] angles with a 22.2 mm [0.875 in] thick bent connection stiffener. Models with finalized cross frame geometry were spot checked against models used to generate influence surfaces. Differences in the skewed-staggered configuration were negligible because maximum stress was located in the positive moment region where non-skewed cross frames were used. Two differences were noted in skewed-parallel configurations. The HSS#1 path was 0.752 mm [0.030 in] closer to the weld toe than in the non-skewed bridge due node locations, which increased HSS approximately 8.8% and a less stiff cross frame assembly was used, which resulted in a HSS magnitude approximately 6.2% lower on average than what would have been generated if finalized cross frame geometry was used. After a detailed investigation it was determined that differences approximately offset each other and no modification was required.

Each bridge deck was divided into a grid of 0.305 m [1.00 ft] squares for loading. A series of 4.45 kN [1.00 kip] loads were applied over an area of 645 mm^2 [1.00 ft^2] and HSSs were extracted from each model. Load placements were minimized by concentrating loads on one half of the bridge and using less dense load placements on the other half to verify symmetry. A total of 400, 258, and 350 load placements were considered for the no-skewed, skewed-parallel, and skewed-staggered bridge configurations respectively.

4.3: RESULTS

4.3.1: MODELS WITH REFINED BOUNDARY CONDITIONS

Preliminary results showed high HSS magnitudes with atypical stress distributions at locations of support, where no differential deflection occurred. Several additional models with unit loads placed to induce maximum demand at the supports were created with highly refined boundary conditions for each bridge configuration. Stress results were compared with initial geometry. Comparison showed stress concentrations in both bottom and top web gaps at supports were artificially inflated due to approximate boundary conditions. Stress concentrations were present at support locations in models with refined boundary conditions, but were much lower than in models with simplified boundary conditions. In addition, maximum HSS magnitudes at supports in models with refined boundary conditions were not as high as HSS in other regions of the bridge. Therefore, HSS at supports were neglected for the remainder of the analysis. More detailed results and plots comparing boundary conditions are presented in Appendix C.

4.3.2: NON-SKEWED BRIDGE

Resulting HSSs from each load placement were used to develop envelope surfaces in addition to influence surfaces. For each load placement analyzed, the maximum HSS magnitude that occurred anywhere in the bridge was used to represent that load placement and results were combined to create the envelope surfaces shown in Figure 5. Results have been mirrored from the northwest (top left) quadrant of the bridge, where the majority of load placements were concentrated. SigmaPlot v11.0 was used to generate contour plots (Systat 2008).

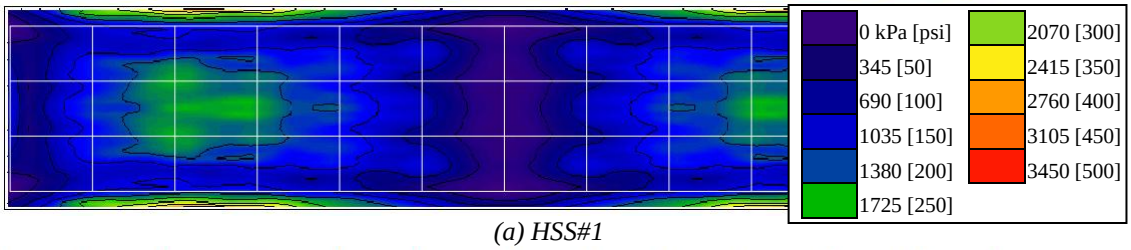

(a) HSS#1

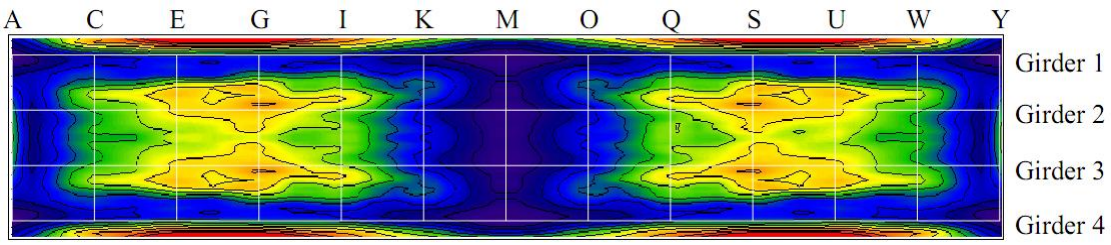

(b) HSS#2

Figure 5: Envelope surfaces for the non-skew bridge

Figure 5 shows that HSS#2 magnitudes were much higher than HSS#1, although HSS#1 details are generally more susceptible to fatigue due to weld quality (Fisher et al. 1990). Loads placed in regions of positive bending, induced the highest HSSs. Critical load placements can be determined from envelope surfaces and include the deck overhang, near the interior girders, and along the bridge centerline. It is unlikely high cyclic loading would occur on the 1.07 m [3.50 ft] wide overhang because of the traffic barrier and roadway shoulder. Therefore, results from loads placed on the overhang are noted herein, but not considered for the remainder of the paper.

Maximum HSS#2 magnitudes occurred in the top web gap on the exterior side of the exterior girders in regions of positive bending and resulted from loads placed near interior girders. The largest HSS#1 magnitudes were produced by loads centered on the bridge or placed near an interior girder; both had similar magnitudes. HSS#1 was largest in the top web gap of the interior side of the exterior girder in regions of positive bending, as illustrated with influences surfaces in Figure 6. Influence surfaces were numbered using the girder number (G1), cross frame row (E), web gap location (top or bottom and north or south, TN), and HSS path (1 or 2). The cross frame to web intersection containing the web gap of interest is circled in the figure.

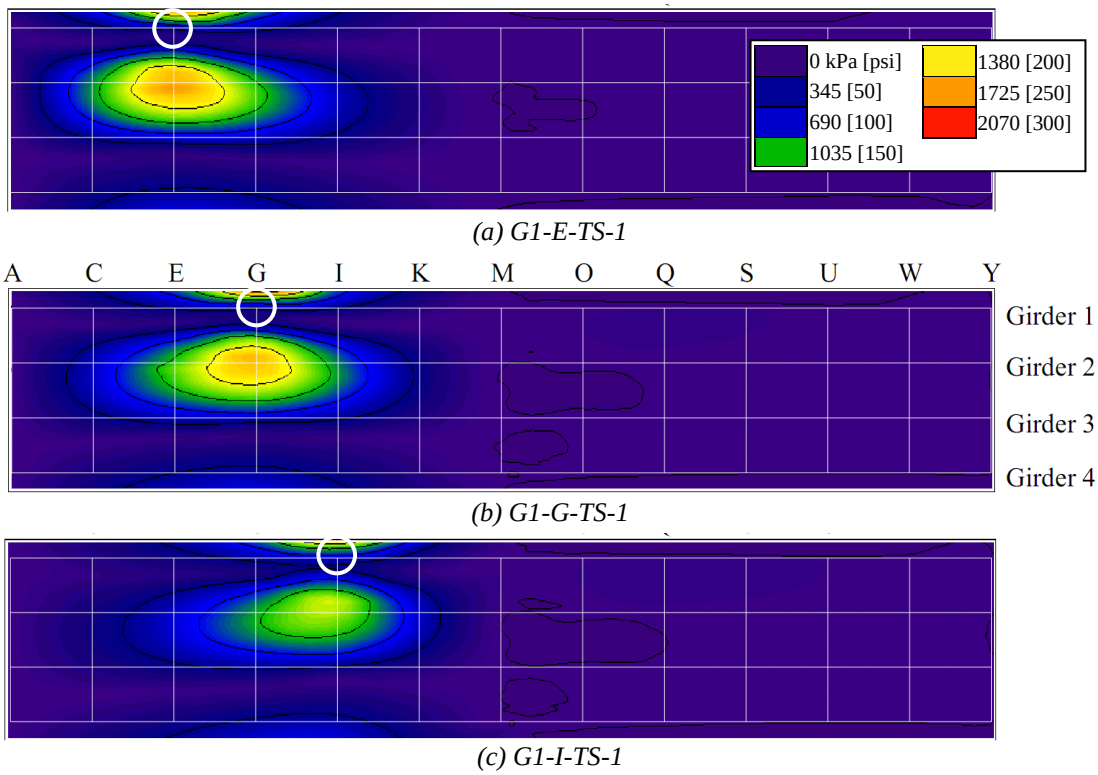

(a) G1-E-TS-1

(b) G1-G-TS-1

(c) G1-I-TS-1

Figure 6: HSS#1 influence surfaces of the non-skewed bridge for the top web gap on the interior side of the north exterior girder in cross frame row (a) E, (b) G, and (c) I

Load placement must be considered relative to the span (region of positive or negative bending), girders, and individual cross frames. Maximum HSS occurred when loads were placed on the bridge deck above the intersection of a cross frame and girder web. Figure 6 shows how load placements inducing maximum stress move with the cross frame row being investigated.

4.3.3: 40 DEG. SKEWED-PARALLEL BRIDGE

Influence surface analysis for the 40 deg. skewed-parallel bridge showed a similar relationship between load placement and location of high web gap stresses. This was expected, as the overall cross frame configuration is very similar, with cross frames placed back-to-back. Maximum stress occurred in top web gaps within the positive moment region due to loads placed in the positive moment region. Loads placed on the deck overhang caused the highest stresses, although theses were again neglected, with the next highest stresses caused by loads placed near interior girders.

An influence surface is presented in Figure 7a for the web gap that had the highest HSS#1 magnitude. Maximum HSS#1 occurred in the top web gap on the interior side of the exterior girder. Maximum stress magnitude was approximately 30% (6895 kPa [100 psi]) higher than the non-skewed bridge. Maximum HSS#2 decreased approximately 10% (345 kPa [50 psi]) from the non-skewed bridge, but also occurred in the top web gap on the exterior side of the exterior girder.

4.3.4: 40 DEG. SKEWED-STAGGERED BRIDGE

In the skewed-staggered bridge, the highest HSS magnitudes resulted from loads placed on the deck overhang, with the second highest magnitudes resulting from load placed near the interior girder; similar to results from the other two bridge configurations. Maximum HSS occurred in the positive moment regions due to loads placed in the positive moment region. Although many similarities were found to exist, results were notably different that the other bridge configurations. The largest HSS#1 magnitude fell in between those that occurred in the non-skewed and 40 deg. skewed-parallel bridge configurations. HSS#1 was highest in the bottom web gap of the loaded, interior girder. As a result, HSS #2 magnitudes were significantly lower than those produced in the non-skewed and skewed-parallel bridge configurations. The cross frame was not pulling on the top web gap as much as when maximum HSS#1 occurred in the top web gap, which reduced the web rotation and subsequent HSS#2 concentration.

High magnitudes of HSS#1 in the bottom web gap are likely due to bottom flange out-of-plane girder movement, which does not occur in bridges with cross frames placed back-to-back. The skewed-staggered configuration forces girders into reverse curvature along the length of the girder. This has also been noted in previous research (Fraser et al. 2000). HSS in the skewed-staggered configuration may also be lower because cross frames are less effective at distributing live loads laterally (Barth and Bowman 2001).

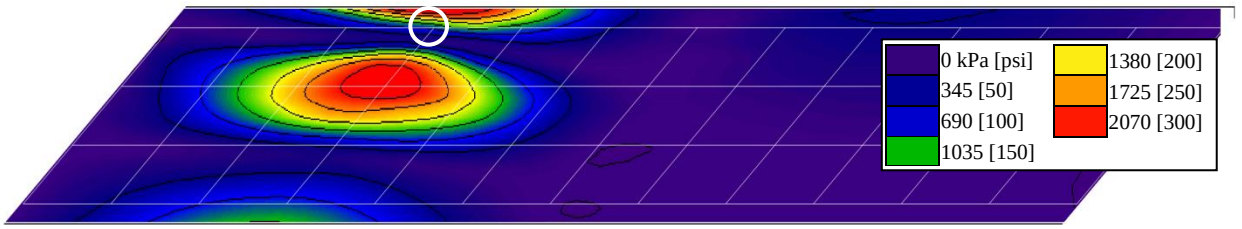

(a) Skewed-parallel bridge, G1-G-TS-1

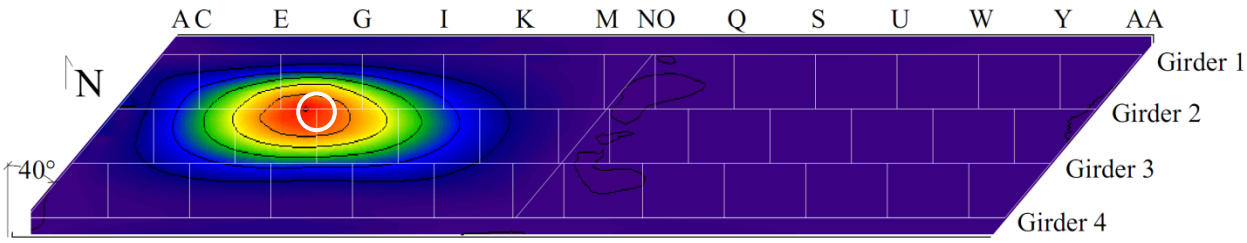

(b) Skewed-staggered bridge, G2-G1-BS-1

Figure 7: HSS#1 influence surfaces for cross frame row G on the (a) top web gap on the interior side of the north exterior girder and (b) bottom web gap on the exterior side of the north interior girder

4.4: Load Placement for Parametric Analysis

From the influence surface analysis it was determined the fatigue truck should be centered over an interior girder in the positive moment region to produce maximum HSS. Girder 2 was selected as the loaded girder because loads placed in the west span over Girder 2, towards the obtuse corner, produced slightly higher stresses in the skewed-staggered bridge than those placed in the west span over Girder 3.

Influence surfaces showed the highest HSS occurred due to loads placed on the bridge deck near a cross frame to girder connection. However, cross frame position was varied significantly (i.e. cross frame spacing and skew angle), so a consistent truck placement routine was developed as follows. In all bridge configurations evaluated, the point of maximum positive moment along the loaded girder (11.0 m [36.0 ft] from either end of the bridge) fell between the two rows of cross frames that produced maximum HSS magnitudes. Accordingly, two truck placements were

considered for each bridge configuration; each centered over a row of cross frames on either side of the point of maximum moment on Girder 2. The fatigue truck was oriented with the front 142 kN [32.0 kip] axle over the cross frame row of interest; directional orientation of the truck (west-facing or east-facing) was chosen in each case to induce the maximum effect. Only results from the truck placement which produced the highest stress magnitude are presented herein.

5: Parametric Analysis of Distortion-Induced Fatigue

After a truck placement procedure was established using influence surface analysis, parametric analysis was conducted on all 60 variations of bridge geometry, each evaluated with two truck placements. In addition, skewed-parallel bridges were modeled with varied cross frame stiffness for a total of 130 FE models.

5.1: Location of Maximum Hot Spot Stress

Location of maximum HSS was noted and compared for each bridge evaluated. Results were similar to those observed during influence surface analysis. Maximum HSS#1 occurred in the top web gap on the interior side of the exterior girder in the positive moment region for the non-skewed, skewed-parallel, and skewed-unstaggered configurations. In bridges with these configurations, HSS#2 was higher than or nearly equal to HSS#1 and maximum HSS#2 occurred in the top web gap on the exterior side of the exterior girder in the positive moment region.

Results for the skewed-staggered configuration were different because cross frames were not placed back-to-back. Stagger allowed more out-of-plane movement near the girder bottom flange as was observed in previous research (Fraser et al. 2000, Barth and Bowman 2001, and Hartman et al. 2010). Maximum HSS#1 occurred in the bottom web gap of the loaded, interior girder in the positive moment region, except for in bridge variations with both large skew angle and cross frame spacing. HSS#2 magnitudes were around 6% (138 kPa [20.0 psi]) lower than HSS#1and occurred in the top web gap on the exterior side of the exterior girder in the positive moment region.

5.2: SKEWED-PARALLEL BRIDGE CONFIGURATIONS

5.2.1: SKEW ANGLE

Results for skewed-parallel configurations are presented in Figure 8 and show the impact of skew angle, cross frame spacing, and cross frame stiffness on both types of HSS. As skew angle increased in bridge models with equal cross frame stiffness, HSS#1 increased and HSS#2 decreased. However, HSS#1 decreased between 30 and 40 deg. skew angles. Cross frame stiffness of the angle/stiffener combination used in 30 deg. skewed models was slightly higher than that used in the 40 deg. skewed models, because stiffener thickness was varied in 3.18 mm [0.125 in] increments. If cross frame stiffness could have been matched exactly, the 40 deg. skewed models would likely have produced a higher HSS#1 magnitude than the 30 deg. skewed bridges.

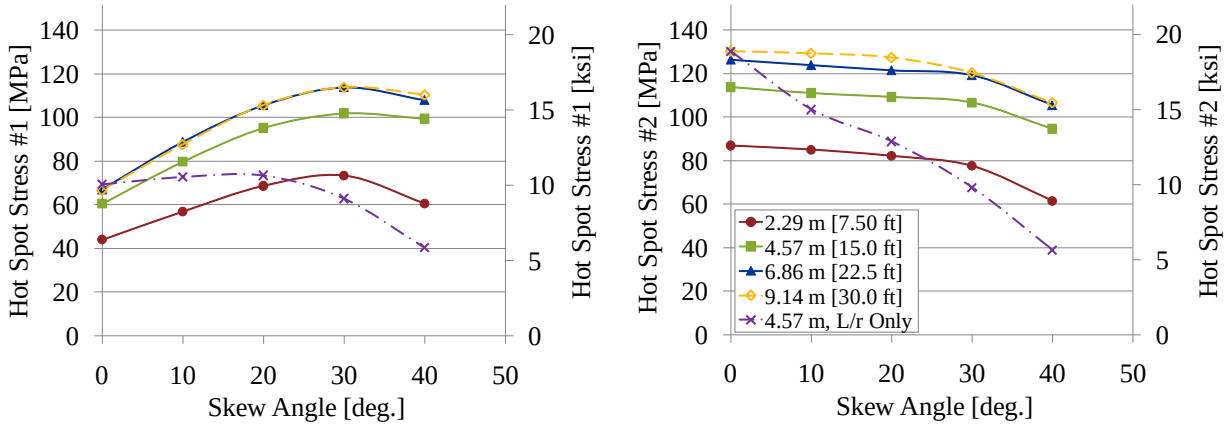

Figure 8: HSS versus skew angle for skewed-parallel bridge configurations for each cross frame spacing evaluated

Skewed-parallel cross frames were selected for stiffness based on lateral forces. In addition to a lateral component, skewed cross frames carry a longitudinal component, parallel to the girder line, as most force is transferred through axial stress. Therefore, the axial force in the cross frames increases with skew angle, which in turn magnifies the resultant force being put on the web gaps and increases HSS#1 as found in previous research (Fisher and Mertz 1984).

5.2.2: CROSS FRAME SPACING

Both HSS magnitudes were higher for bridges with large cross frame spacing, as illustrated in Figure 8. As spacing becomes larger and cross frames are removed, the remaining cross frames must distribute a larger portion of the load, increasing force and HSS in the remaining cross

frames. However, stress change was not consistent for each increase in spacing. Change was most significant when spacing increased from 2.29 to 4.57 m [7.50 to 15.0 ft], but almost negligible when spacing increased from 6.86 to 9.14 m [22.5 to 30.0 ft]. This shows the cross frames have an upper limit of effectiveness, and cannot distribute much additional live load beyond that carried in models with 6.86 [22.5 ft] spacing.

Previous versions of the AASHTO (2004) specification have limited cross frame spacing to 7.62 m [25.0 ft], but this provision has been removed in lieu of performing a rational analysis (2007). Many state DOTs still adhere to this limit although it has been changed (IlDOT 2009, IoDOT 2010, KDOT 2010, and WDOT 2002). Results from models evaluated in this study suggest that in some bridge configurations, 7.62 m [25.0 ft] may be a reasonable upper limit for effective cross frame spacing based on the live load distribution, because similar HSS magnitudes were found in bridges with 6.86 and 9.14 m [22.5 and 30.0 ft] cross frame spacing.

Results highlight that cross frame spacing should be carefully selected. Large cross frame spacing minimizes the number of fatigue prone details present, but may increase susceptibility of each detail to distortion-induced fatigue. This should also be considered when cross frames are removed as a retrofit procedure.

5.2.3: CROSS FRAME STIFFNESS

Skew angle and cross frame spacing influence susceptibility of bridges to distortion-induced fatigue; however, cross frame stiffness has an equally significant effect though more frequently neglected. Cross frame stiffness was given careful consideration in this parametric study, and angle/stiffener combinations were chosen at approximately equal levels of stiffness. However, the angle/stiffener combinations used herein are much larger than likely to been seen in the field based on review of some state DOT bridge design manuals and standard details (CDOT 2009, IoDOT 2010, KDOT 2010, TxDOT 2009, and WDOT 2002). To illustrate the effects of cross frame stiffness on distortion-induced fatigue, an additional set of cross frame angle/stiffener combinations, more representative of standard practice, were chosen.

It is the opinion of the author that provisions adopted by some state DOTs do not give adequate consideration to cross frame stiffness, which includes stiffness of both the cross frame members and connection stiffeners, especially in bridges with large skew angles. Some design provisions

advise that angle sizes be selected based primarily or solely on slenderness requirements and many do not consider skew angle beyond its contribution to increased cross frame length (CDOT 2009, KDOT 2010). Furthermore, provisions do not address the effects of the flexibility of the connection on the stiffness of the cross frame assembly, which as previous research has shown, can be very significant (Yura 2001).

Accordingly, a smaller set of cross frames was selected based on L/r requirements only. L127x127x7.94 mm [L5.00x5.00x0.3125 in] angles were used for the 0 deg. to 30 deg. bridge configurations and L152x152x9.53 mm [L6x6x0.375 in] angles were used in the 40 deg. bridge. Only skewed-parallel bridges with cross frames spaced at 4.57 m [15.0 ft] were evaluated with "L/r only" cross frame sizes. Stiffeners were sized to meet projecting width and moment of inertia limitations only, therefore did not change as cross frames lengthened. A 9.52 x 127 mm [0.375 x 5.00 in] stiffener was used in the non-skewed bridge and was lengthened to 152 mm [6.00 in] when the bent plate stiffener was used in skewed configurations.

It is recognized that connection stiffeners used at points of support would likely be much larger in practice than intermediate stiffeners, as bearing stiffeners are designed for high web strength demands. However, bridges with "L/r only" cross frames used the same angle/stiffener combinations for cross frames throughout the bridge to maintain consistency between all models. The authors would expect to see some increase in HSS concentrations at these locations if more substantial stiffeners were used, especially in cases of large cross frame spacing and/or staggered bridge configurations. It is also possible that one reason for conflicting results regarding locations of cracking reported in the literature is due to varied cross frame stiffness throughout the bridge.

The significant impact that cross frame stiffness has on web gaps stress is illustrated in Figure 8. Results show that cross frame stiffness is an important, though frequently overlooked parameter, which had an equally significant effect on HSS as other parameters investigated. HSS#1 in bridges with "L/r only" cross frame sizes did not increase with skew as predicted. As skew angle increases bracing becomes significantly less stiff and less effective. Implications of neglecting cross frame stiffness are important from a distortion-induced fatigue perspective, but also noteworthy from a broader perspective. Previous research by Yura and Helwig (2001; 2008) has focused the importance of considering brace and connection stiffness from a more general

stability standpoint. Therefore, brace stiffness should be selected with care to ensure brace sizes are adequate to stabilize girders and distribute lateral loads, but not overly stiff to avoid increasing distortion-induced fatigue susceptibility. Cross frame stiffness and its effect on distortion-induced fatigue susceptibility are described in detail in Appendix A.

5.3: Skewed-Unstaggered Bridge Configurations

Results from skewed-unstaggered bridge configurations are presented in Figure 9. HSS#2 magnitudes were over two times larger than HSS#1 magnitudes. Therefore, cracking seems most likely to occur at the flange to web intersection (HSS#2) because of the significant stress difference, even though it occurs at a less fatigue-susceptible detail (Fisher et al. 1990; AASHTO 2007). Both HSS#1 and HSS#2 remained approximately constant for all skew angles evaluated. Increasing cross frame spacing amplified HSS; however magnitudes were similar for models with cross frames spaced at 6.86 m [22.5 ft] and 9.14 m [30.0 ft].

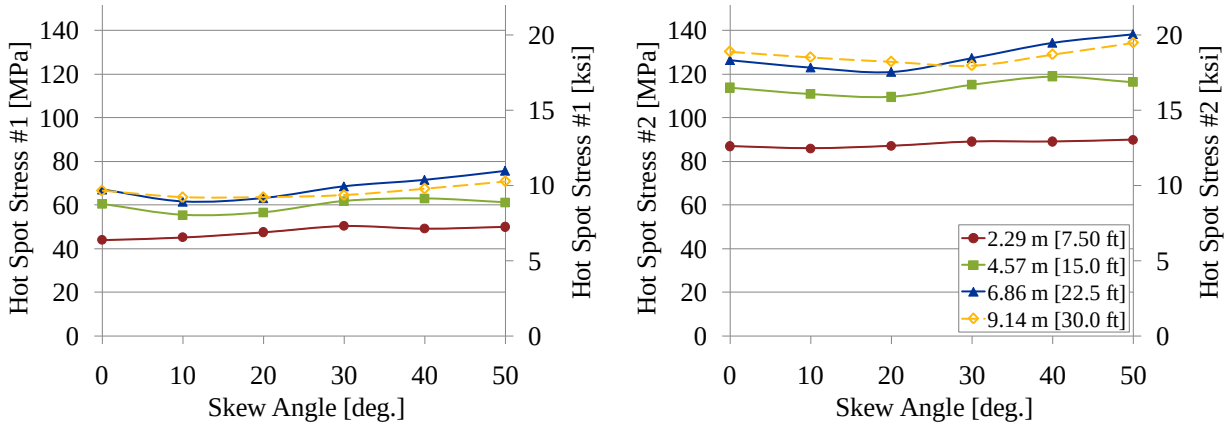

Figure 9: HSS versus skew angle for skewed-unstaggered bridge configurations for each cross frame spacing evaluated

5.4: Skewed-Staggered Bridge Configurations

Skew angle and cross frame spacing had a less significant effect on resulting stresses in skewed-staggered configurations than the other bridge configurations evaluated, except in bridges with both large skew angle and cross frame spacing. Results are presented in Figure 10, and show HSS varied moderately between bridge variations evaluated.

Overall, out-of-plane girder response and stiffness, which was influenced by skew angle and cross frame spacing, controlled bridge behavior in skewed-staggered configurations. The girder

bottom flange deflected out-of-plane in response to differential deflection, out-of-plane girder stiffness, amount and position of bracing, and cross frame forces being distributed through the girder web because cross frames are not placed back-to-back (Fraser et al. 2000; Hartman et al. 2010). Systems with large out-of-plane deflections cannot distribute loading through interior cross frames efficiently (Barth and Bowman 2001). Skew angle and cross frame spacing influenced out-of-plane girder response in the following ways:

- Increased cross frame spacing amplifies cross frame forces and induces larger out-of-plane movement of girders.
- Increased cross frame spacing decreases the out-of-plane girder restraint, which allows girders to move more easily.
- Increased skew angle magnifies potential differential deflections due to the difference in stations at which either end of the cross frame are attached.
- Increased skew angle makes the distance between staggered cross frames in the same row, along the girder web larger (increases the degree of stagger).

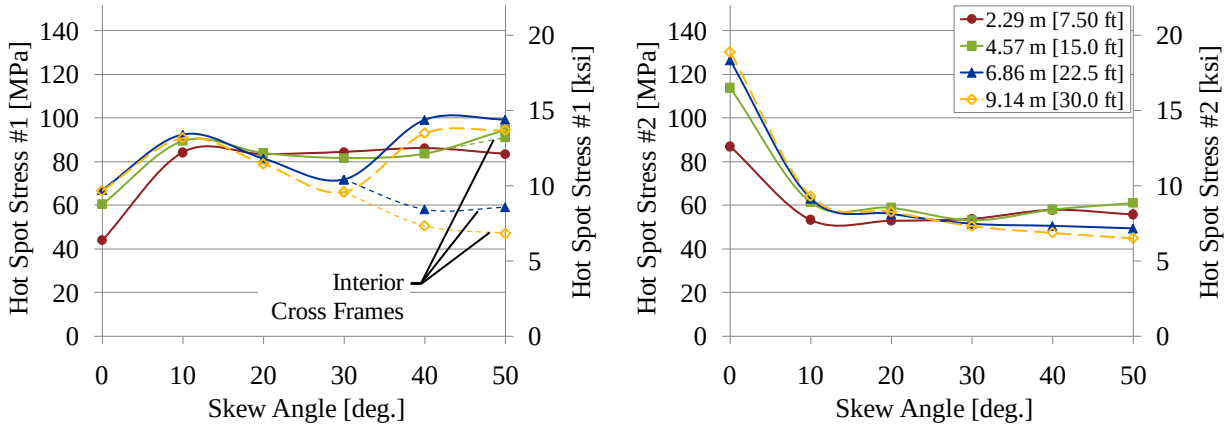

Figure 10: HSS versus skew angle for skewed-staggered bridge configurations for each cross frame spacing evaluated

Intermediate cross frames were less effective in bridges with large skew angle and cross frame spacing large out-of-plane girder response and led to a shift in the location of maximum HSS#1. For these models HSS#1 at interior cross frames are shown in Figure 10 in addition to maximum stresses in the bottom web gap of the loaded girder at the abutment. Maximum HSS#1 stress shifted to supports, as cross frames were placed back-to-back at these locations. HSS#1 magnitudes were relatively high in these cases because all lateral load was distributed at supports. Additional models with refined boundary conditions were used to verify HSS

magnitudes because boundary conditions were applied at girder ends, where maximum stresses occurred.

5.5: Comparison of Bridge Configurations

Results for all configurations were plotted together and grouped by cross frame spacing, so relative distortion-induced fatigue susceptibility could be more easily compared. Figure 11 shows results for models with cross frames spaced at 4.57 m [15.0 ft]. Skewed-unstaggered configurations had the lowest HSS#1 magnitudes, excluding the more realistic skewed-parallel models with low cross frame stiffness. However, HSS#2 was highest in skewed-unstaggered configurations, highlighting the importance of considering both stress types when evaluated risk of distortion-induced fatigue.

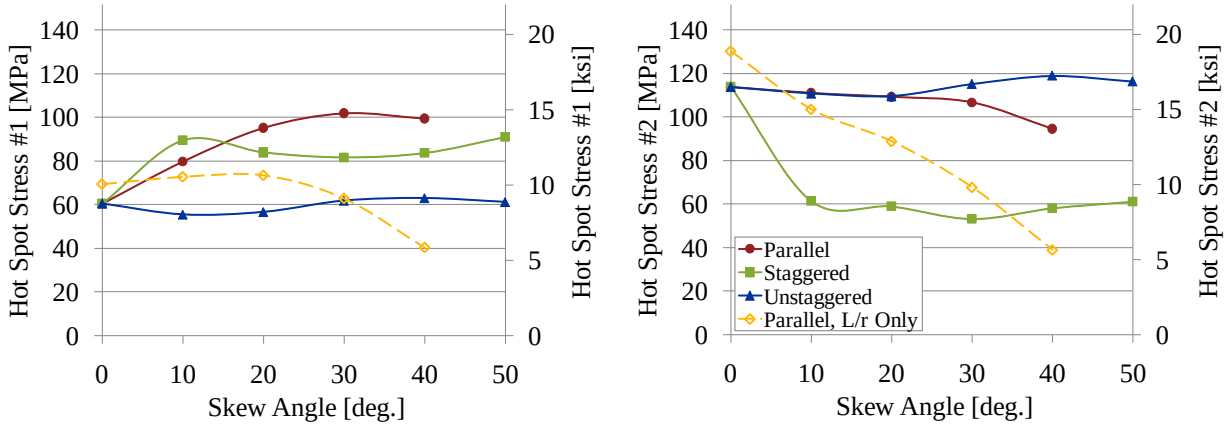

Figure 11: HSS versus skew angle for configurations with a 4.57 m [15.0 ft] spacing

In bridges with 4.57 m [15.0 ft] cross frame spacing, HSS was higher in skewed-parallel bridges than in skewed-staggered bridges. This is contrary to the general theory that skewed-parallel bridge configurations are less susceptible to distortion-induced fatigue, because cross frames are attached to the same point of adjacent girders, decreasing potential differential deflection. AASHTO (2007) does not recommend the use of skewed-parallel configurations in bridges with skew angles greater than 20 deg., but some states use this configuration well beyond the 20 deg. limit to reduce risk of distortion-induced fatigue (KDOT 2010). However, results suggest that in skewed-parallel configurations that utilize cross frames with lateral stiffness equal to that of the non-skewed cross frame, skewed-staggered bridges may be less susceptible to distortion-induced fatigue than skewed-parallel bridges. It is important to note than many states do not use skewed cross frames with equal stiffness, as previously discussed, and models with "L/r only" cross

frame sizes had lower HSS#1 magnitudes than either the skewed-staggered or skewed-parallel configurations.

Relative HSS#2 magnitudes were similar for all cross frame spacing evaluated with skewed-staggered bridge configurations producing the lowest stresses. HSS#1 also had similar relative values for all cross frame spacings except 2.29 m [7.50 ft]. Skewed-staggered bridges had higher HSS#1 than skewed-parallel bridges for models with cross frames spaced at 2.29 m [7.50 ft].

6: CONCLUSIONS

The parametric study described herein evaluated the effects of skew angle, cross frame spacing, bracing configuration, cross frame stiffness, and load placement on bridge susceptibility to distortion-induced fatigue as quantified by hot spot stresses. Over 1000 detailed, finite element models were used in this investigation. Conclusions can be summarized as follows:

- Stiffness of both cross frame elements and connection stiffeners had a significant impact on bridge susceptibility to distortion-induced fatigue and should be considered as important as other evaluated parameters including skew angle and cross frame spacing. Increased stiffness of these element corresponded with increased hot spot stress.
- In skewed-parallel bridges, especially those with large skew angles (of 40 degrees or greater), neglecting the stiffness of either the cross frame element or connection could lead to proportioning of cross frames that are significantly more flexible than similarly proportioned cross frames in non-skewed bridges..
- Relative bracing stiffness within a bridge may control the region of the bridge most likely to develop distortion-induced fatigue cracking. This may be one reason previous literature presents conflicting conclusions regarding the region of the bridge most vulnerable to distortion-induced fatigue.
- Maximum hot spot stress magnitudes occurred in top web gaps in regions of positive bending when cross frames were placed back-to-back, but occurred in bottom web gaps of skewed-staggered bridges.
- Two distinct types of stress concentration occurred in the web gap region; hot spot stress at the connection stiffener to web weld (HSS#1) and at the flange to web weld (HSS#2).

Both are important to consider separately, as relative importance may be dependent on local web gap geometry.

- In skewed-parallel bridges, the magnitude of stress concentration at the web to stiffener weld (HSS#1) increased with skew angle, while the stress concentration at the web to flange weld (HSS#2) decreased with skew angle. Skew angle did not have a significant impact on hot spot stress in skewed-unstaggered bridges.
- Cross frame spacing in non-skewed, skewed-parallel, and skewed-unstaggered bridges increased hot spot stress at both weld locations (HSS#1 and HSS#2), although magnitudes were similar for bridges with cross frames spaced at 6.86 m [22.5 ft] and 9.14 m [30.0 ft].
- Out-of-plane girder response and stiffness significantly affected hot spot stress magnitudes in skewed-staggered bridge configurations due to out-of-plane girder movement. Stress fluctuated in magnitude and location based on out-of-plane girder response rather than cross frame spacing or skew angle directly.

DOTs across the country are working to inspect, repair, and retrofit bridges which have developed or are susceptible to distortion-induced fatigue cracking. It is important to understand and quantify the effects of skew angle, cross frame spacing, bracing configuration, and cross frame stiffness on distortion-induced fatigue so that at-risk bridges and regions within those bridges where cracks are most likely to occur can be identified and inspected. In addition, understanding parameters associated with distortion-induced fatigue will help develop effective repair and retrofit techniques that will not create unforeseen fatigue problems in the future.

7: REFERENCES

AASHTO (2007). "LRFD Bridge Design Specifications." *American Association of State Highway and Transportation Officials*, Washington, D.C.

AASHTO (2004). "LRFD Bridge Design Specifications." *American Association of State Highway and Transportation Officials*, Washington, D.C.

AISC (2005). "Steel Construction Manual, 13th Ed." *American Institute of Steel Construction*, Chicago, IL.

AISI Example 2: Two-Span Continuous Composite I Girder (1997). *American Iron and Steel Institute*.

Barth (Grider), A.S. and Bowman, M.D. (2001). "Fatigue Behavior of Welded Diaphragm-to-Beam Connections." *Journal of Structural Engineering*, 127(10), 1145-1152.

Barth, K.E., Hartnagel, B.A., White, D.W., and Barker, M.G. (2004). "Recommended Procedures for Simplified Inelastic Design of Steel I-Girder Bridges." *Journal of Bridge Engineering*, 9(3), 230-242.

Berglund, E. and Schultz, A. (2006). "Girder Differential Deflection and Distortion-Induced Fatigue in Skewed Steel Bridges." *Journal of Bridge Engineering*, 11(2), 169-177.

Castiglioni, C.A.; Fisher, J.W.; and Yet, B.T. (1988). "Evaluation of Fatigue Cracking at Cross Diaphragms of a Multigirder Steel Bridge." *Journal of Constructional Steel Research*, 9(2), 95-110.

CDOT. (2009). "Bridge Design Manual." *Colorado Department of Transportation*.

Connor, R.J. and Fisher, J.W. (2006). "Identifying Effective and Ineffective Retrofits for Distortion Fatigue Cracking in Steel Bridges Using Field Instrumentation." *Journal of Bridge Engineering*, 11(6), 745-752.

Fisher, J. W., Barthelemy, B. M., Mertz, D. R., and Edinger, J. A. (1980). "Fatigue Behavior of Full-Scale Welded Bridge Attachments." *National Cooperative Highway Research Program Report #227*, Transportation Research Board, National Research Council, Washington, D.C.

Fisher, J. W., Jian, J., Wagner, D. C., and Yen, B. T. (1990). "Distortion-Induced Fatigue Cracking in Steel Bridges." *National Cooperative Highway Research Program Report #336*, Transportation Research Board, National Research Council, Washington, D. C.

Fisher, J. W. and Mertz, D. R. (1984). "Fatigue and Fracture in Steel Bridges." *The Conference on Bridges*, Pittsburgh, PA, 10-21.

Fraser, R.E.K., Grondin, G.Y., and Kulak, G.L. (2000). "Behavior of Distortion-Induced Fatigue Cracks in Bridge Girders." *Structural Engineering Report No. 235*.

Hartman, A., Hassel, H., Adams, C., Bennett, C., Matamoros, A., and Rolfe, S. (2010). "Effects of Cross-Frame Placement and Skew on Distortion-Induced Fatigue in Steel Bridges." *Transportation Research Record* (TRR), 2200, 62-68.

IlDOT. (2009). "Bridge Manual." *Illinois Department of Transportation Bureau of Bridges and Structures*.

IoDOT. (2010). "LRFD Bridge Design Manual." *Iowa Department of Transportation Office of Bridges and Structures*.

Jajich, D. and Schultz, A.E. (2003). "Measurement and Analysis of Distortion-Induced Fatigue in Multigirder Steel Bridges." *Journal of Bridge Engineering*, 8(2), 84-91.

KDOT. (2010). "Design Manual: Volume III – Bridge Selection." *Kansas Department of Transportation*.

Khalil, A., Wipf, T.J., Greimann, L., Wood, D.L., and Brakke, B. (1998). "Retrofit Solution for Out-of-Plane Distortion of X-Type Diaphragm Bridges." *Transportation Conference Proceedings, Iowa Department of Transportation*, 99-102.

Li, H. and Schultz, A. E. (2005). "Analysis of Girder Differential Deflection and Web Gap Stress for Rapid Assessment of Distortional Fatigue in Multi-Girder Steel Bridges." *Final Report 2005-38*, Minnesota Department of Transportation, St. Paul, MN.

Roddis, W.M.K. and Zhao, Y. (2001). "Out-of-Plane Fatigue Cracking in Welded Steel Bridges: Why It Happened and How It Can Be Repaired." *Welding Innovation*, 27(2), 2-7.

Simulia. (2008). ABAQUS FEA Version 6.8.2. Providence, RI. http://www.simulia.com

Systat Software, Inc. (2008). SigmaPlot 11.0.0.75. http://www.systat.com

TxDOT. (2009). "Bridge Design Manual – LRFD." *Texas Department of Transportation*.

Wang, L. and Helwig, T.A. (2008). "Stability Bracing Requirements for Steel Bridge Girders with Skewed Supports." *Journal of Bridge Engineering*, 13(2), 149-157.

Wisconsin Department of Transportation (WDOT). (2002). "Bridge Manual." *WDOT*.

Yura, J. (2001). "Fundamentals of Beam Bracing." *Engineering Journal*, AISC, First Quarter, 11-26.

Zhao, Y. and Roddis, W. M. K. (2003) "Finite Element Study of Distortion-Induced Fatigue in Welded Steel Bridges." *Transportation Research Record*, 1845, 57-65.

APPENDIX A: CROSS FRAME STIFFNESS WITH RESPECT TO DISTORTION-INDUCED FATIGUE

A.1: PROBLEM STATEMENT

Initial objectives of the parametric analysis were to determine the effects of skew angle, cross frame spacing, and bracing configuration on distortion-induced fatigue. However, bridge geometry necessitated investigation of an additional parameter, cross frame stiffness, which was determined to have an equally significant impact on distortion-induced fatigue.

Skewed-parallel cross frames are longer and require different connections than cross frames oriented perpendicular to the girder. As cross frames lengthen, they become less stiff and less effective at distributing forces between girders if the same connecting elements are used. Also, bent plate stiffeners are used in skewed bridges to facilitate welding during construction. Geometric change resulting from bridge configuration and skew angle are shown in Figure A.1. A detailed investigation of the effects of these geometric changes on cross frame stiffness was conducted to select cross frame and stiffener sizes for each bridge configuration evaluated.

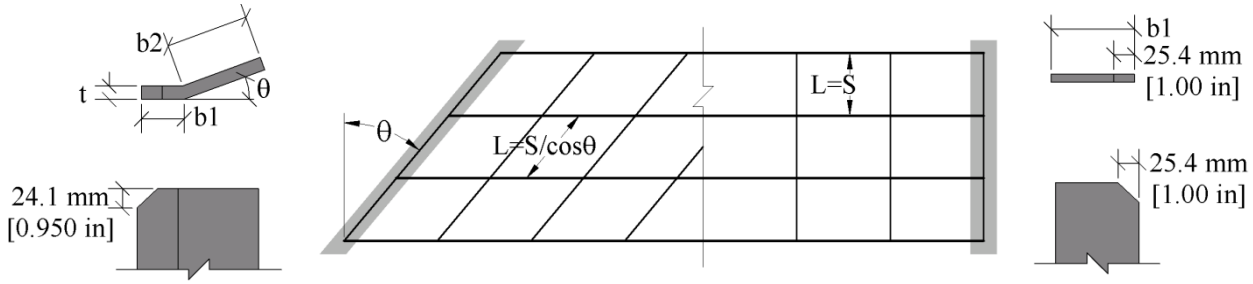

(a) Bent plate stiffener *(b) Cross frame orientations* *(c) Non-skewed stiffener*

Figure A.1: Geometric changes for skewed-parallel cross frames

The objective of the cross frame sub-modeling was to determine the appropriate size of cross frame elements and connection stiffeners (angle/stiffener combinations) to maintain an approximately equal level of stiffness in bridges with varied skew angle. By holding cross frame stiffness approximately constant between models, the effects of skew angle, cross frame spacing, and bracing configuration on distortion-induced fatigue could be more clearly evaluated. Then, cross frame stiffness was deliberately varied to analyze its effects on web gap stresses associated with distortion-induced fatigue.

A.2: BACKGROUND

A.2.1: BEAM BRACING

In most multi-girder bridges, cross frames or diaphragms are used as stability bracing for girders before the concrete deck has cured and composite action can be established. Cross frames, which were used in this study, are classified as nodal (discrete) torsional bracing, meaning they control girder rotation at a single point along the girder. Once the deck has cured, bracing at support locations continue to play a significant role in distributing lateral forces, but contributions from interior bracing is no longer as significant. Though interior braces are not a highly-significant part of the primary lateral load resisting system once the concrete deck is in place, they do help distribute live loads laterally. Furthermore, the behavior of cross frames subjected to differential deflections is the primary cause of distortion-induced fatigue and therefore an important part of this investigation.

A.2.2: CROSS FRAME STIFFNESS

Stiffness of cross frame configurations can be determined using elastic truss analysis. The frame is idealized and subjected to moment *M*, induced by a pair of forces *F* as shown in Figure A.2a. Stiffness is computed by dividing the moment by resulting rotation, θ. Figure A.2 defines stiffness of three common types of cross frames. A tension system requires horizontal members, but only two members are acting for one direction of force (denoted by bold lines). Horizontal members are not required in a tension-compression system. In a K-Brace system, diagonals must be designed for tension and compression and the top horizontal member is not required. X-type, tension-compression bracing was used in this study.

A.2.3: CONNECTION STIFFNESS

Susceptibility of a braced cross-section to distortion can limit effectiveness for both lateral and torsion bracing as reflected in Equation A.1 (AISC 2005). Bracing system stiffness (β_{act}) will be less than the smaller of the brace stiffness (β_{br}) and the connection stiffness (β_{conn}). The element with the smallest stiffness will control stiffness of the assembly; therefore cross-sectional distortion has a significant potential impact on effectiveness of torsional bracing (Yura 2001). In addition to the stiffener itself, many state DOTs use partial depth gusset plates to attach cross frame elements to connection stiffeners as shown in Figure A.3. Stiffness of gusset plates should

also be considered, although connection between cross frame elements and connection stiffeners are made directly in this investigation.

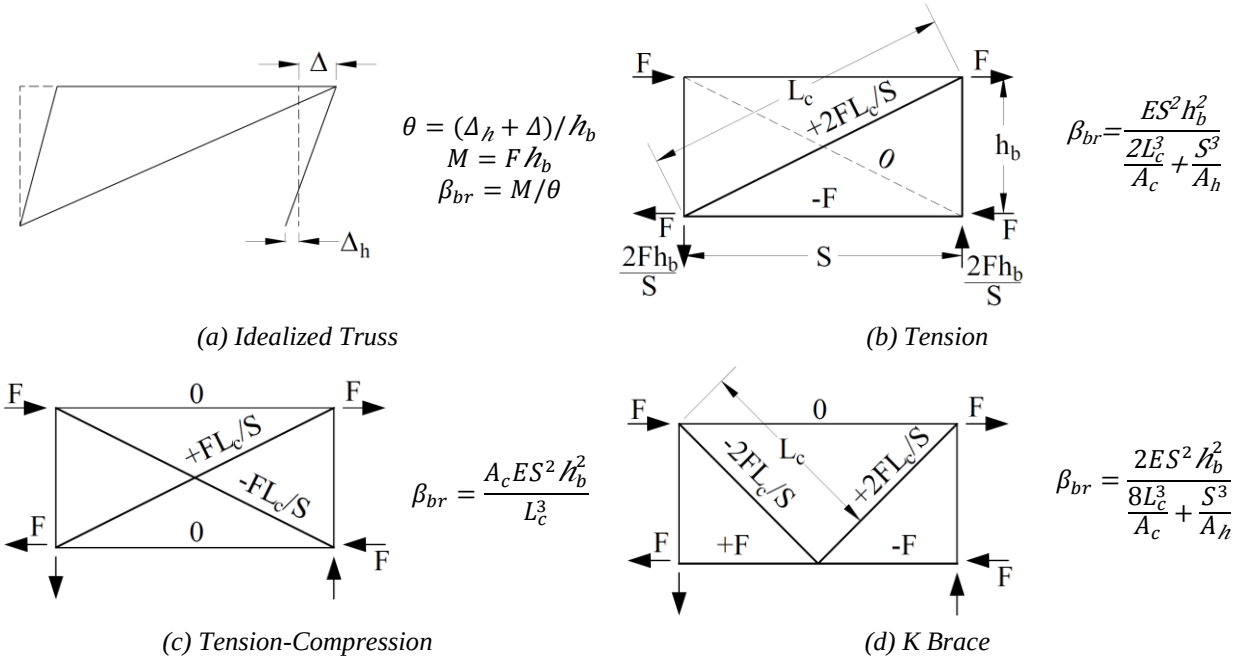

Figure A.2: Cross frame stiffness (Yura 2001)

Web stiffness may be separated into several parts to account for partially stiffened webs as shown in Figure A.3 (Yura et al. 1992). Total web height may include an unstiffened portion adjacent to the top flange (h_c), a stiffened portion (h_s), and an unstiffened portion adjacent to the bottom flange (h_t). Stiffness of each portion is computed using Equation A.2 (subscript *i* is used here to denote each portion of the web). Then reciprocals are summed to determine the connection stiffness using Equation A.3. The equation can be further refined such that h_b is considered infinitely stiff.

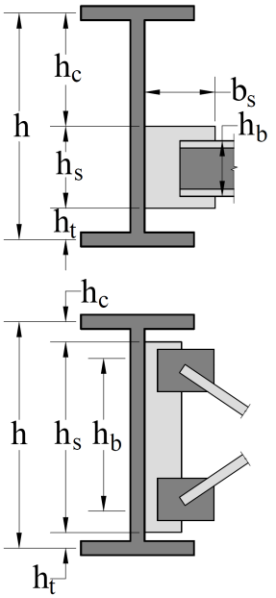

Figure A.3:Web stiffness

$$\frac{1}{\beta_{act}} = \frac{1}{\beta_{conn}} + \frac{1}{\beta_{br}} \qquad \textit{Equation A.1}$$

$$\beta_i = \frac{3.3E}{h_i}\left(\frac{h}{h_i}\right)^2\left(\frac{1.5h_i t_w^3}{12} + \frac{t_s b_s^3}{12}\right) \quad i \textit{ equals c, s, or t} \qquad \textit{Equation A.2}$$

$$\frac{1}{\beta_{conn}} = \sum\frac{1}{\beta_i} = \frac{1}{\beta_g} + \frac{1}{\beta_c} + \frac{1}{\beta_s} + \frac{1}{\beta_t} \qquad \textit{Equation A.3}$$

A.2.4: SKEWED CROSS FRAMES

When bracing members are not placed perpendicular to the braced member, additional considerations are required. Both brace stiffness and strength are affected by skew angle. Although modifications have been developed geometrically and used in design, an analytical investigation was recently conducted by Wang and Helwig (2008) to verify this common practice (Yura et. al. 1992).

Stiffness is modified by as shown in Equation A.4. It is important to note that brace stiffness itself will also decrease due to skew because the brace is longer than it would be in the non-skewed condition. These modifications do not account for skew effects on cross-sectional distortion, which is an important limitation for torsional bracing. Research is currently in progress to determine the effects of bent or skewed connection stiffeners on bracing stiffness at the University of Texas, Austin.

$$\beta_{br,skew} = \beta_{br} cos^2\theta \qquad \textit{Equation A.4}$$

A.3: MODELING METHODOLOGY

A.3.1: BRIDGE GEOMETRY

To study the effects of skewed cross frames in a computationally efficient manner, sub-models were created which consisted of three, 9.14 m [30.0 ft] girders, spaced 3.05 m [10.0 ft] apart. Girders were simply supported and connected by three rows of cross frames spaced every 4.57 m [15.0 ft] as shown in Figure A.4a. Models were constructed with 0, 10, 20, 30, 40, 50, and 60 deg. skew angles and a variety of equal leg angles and stiffeners. Bridges were loaded on the top flange of the middle girder at the centerline of the span and resulting forces in the brace members at the span centerline were recorded. A concrete deck was not used in the sub-models as isolated effects of cross frame behavior were desired.

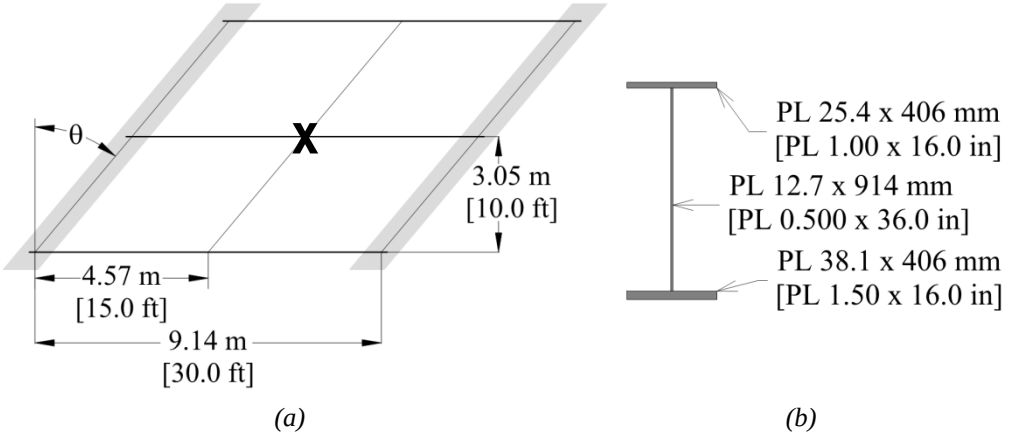

Figure A.4: Sub-modeling geometry

Girder dimensions were adapted from the American Iron and Steel Institute (AISI), Design Example 2 (1997) as this geometry was used in full bridge models for parametric analysis. Cross-sectional dimensions were those used in the negative moment region of the full bridge models and are presented in Figure A.4b.

A.3.2: Cross Frame Geometry

Cross frame geometry for both the non-skewed bridge and skewed bridge are shown in Figure A.5. Angle sizes not included in the AISC Manual (2005) were considered due to the sensitivity of stiffness parameters and need to match the stiffness of the cross frames as closely as possible. Equal leg angle selection was made by matching both slenderness ratio and stiffness.

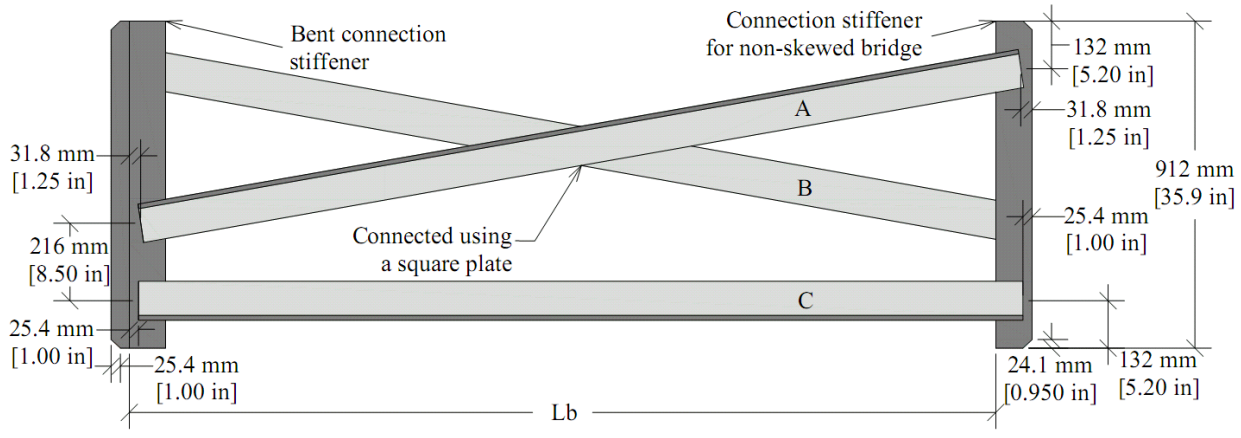

Figure A.5: Cross frame geometry

Slenderness ratio was determined using provisions of AISC, Section E5 (2005). A maximum allowable slenderness of 140 for tension-compression type cross frames is specified by AASHTO (2007) and used during design by many state DOTs. Unbraced length of the cross

frame (L_b) was determined using Equation A.5 where *S* is the girder spacing *(S = 3,048 mm [120 in]),* t_w is the web thickness (t_w*=12.7 mm [0.500 in]*), b_1 is the connection stiffener width perpendicular to the web (b_1, mm [in]), and θ is the skew angle (deg.). An L108x108x12.7 mm [L4.25x4.25x0.500 in] angle was chosen for the non-skewed bridge, because it had a slenderness ratio closest to, but less than 140.

$$L_b = (S - t_w - 2 \cdot b_1)/cos\theta \qquad \textit{Equation A.5}$$

Cross frame stiffness was determined in accordance with Equation A.6 where *A* is the cross-sectional area of the brace (mm^2 [in^2]), *E* is the elastic modulus (MPa [ksi]), *L* is the unbraced length of member C (mm [in]), h_b is the height of the brace (mm [in]), L_c is the length of the diagonal member (A or B, mm [in]), and θ is the bridge skew angle (deg.).

$$\beta = \frac{AEL^2h_b^2}{L_c^3}cos^2\theta \qquad \textit{Equation A.6}$$

By assuming L_c is approximately equal to *L*, *L* is equal to $Scos\theta$, and removing the constant terms (including *E, S,* and h_b), the required cross-sectional area for angles used in skewed bridges can be determined using $Acos^3\theta$. Accordingly, angles for the skewed bridges were chosen by finding a slenderness ratio less than 140 and an $Acos^3\theta$ closest to that of the non-skewed bridge. Angle selections for each skew angle along with unbraced length, slenderness ratio, and stiffness are given in Table A.1.

Angle slenderness and cross-sectional area required for the 50 and 60 deg. skewed bridge were very large and were considered unrealistic as the maximum available angle size is an L203x203x28.6 mm [L8.00x8.00x1.125 in], and an angle much larger would be required to match stiffness of the non-skewed bridge. A WT could be used in place of an angle, but the differences in stiffness and geometry were considered too large of unknowns to make the additional data point meaningful. Therefore, the 60 deg. skew angle was not considered in the remainder of the sub-modeling for parametric analysis. The 50 deg. skewed cross frame utilized the same angle cross section as the 40 deg. skewed cross frame, and did not have equal stiffness to the other angle/stiffener combinations. It was only used in skewed-staggered and skewed-unstaggered bridge configurations.

Because stiffness of skewed and bent connection stiffeners is not well-understood the effects of thickening and lengthening the connection plates were investigated analytically to determine stiffener sizes to be used for the parametric study.

A.3.3: FINITE ELEMENT MODELING

A finite element model of the reduced version of the bridge was constructed in Abaqus v6.8.2 using three dimensional elements (Simulia 2008). Each model consisted of around 320,000 total elements. Element types, mesh sizes, and elastic material properties were the same as those used in the parametric analysis and are described in Section 3.3. Welds were not used to connect parts in sub-models. Instead, flanges and cross frames were tied directly to the girder web. A load of 26.7 kN [6.00 k] was applied over an area of 1,935 mm^2 [3.00 in^2] centered over the center of the middle girder. The load was chosen to induce approximately the same magnitude of differential deflection observed in the full bridge model of the 40 deg. skewed-staggered bridge, 1.27 mm [0.050 in]. Translational restraint was applied at the ends of the girder over and 152 mm [6.00 in] long section of the bottom flange. An overview of the finite element model is shown in Figure A.6.

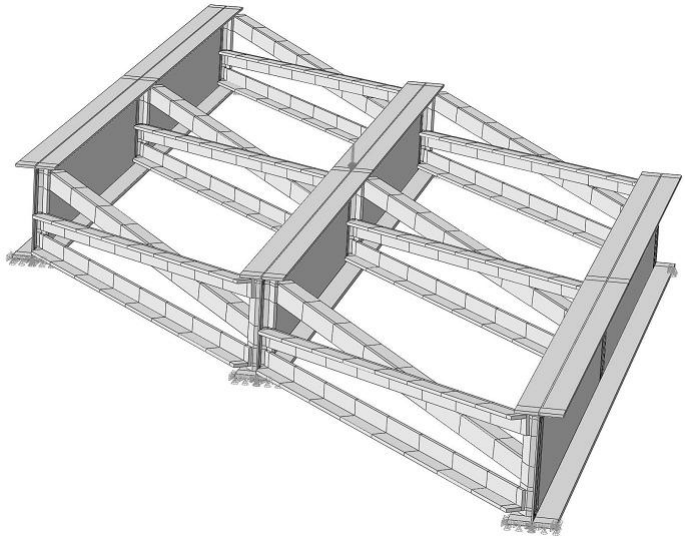

Figure A.6: Overview of finite element model

A.3.3: CROSS FRAME FORCES

Each cross frame member was partitioned at seven equally spaced places along the length of the angle. The free body cut tool was utilized to determine the resultant forces and moments acting at each section. Some moment was developed in braces, but axial forces were considered most

important when determining cross frame stiffness. Forces at each section were averaged to quantify axial force in each member. Then lateral forces were determined using bridge skew angle and results were compared to those developed in other bridges configurations to determine stiffener geometry to be used for the parametric analysis.

A.4: RESULTS

A.4.1: STIFFENER LENGTH

The stiffness contribution of the connection stiffener was evaluated by varying both stiffener length and thickness. Total length of the bent plate stiffener was composed of a portion perpendicular to the girder line (b_1) and a portion parallel to skew angle (b_2). Each portion of the bent plate stiffener was varied individually to determine the effect on the amount of axial force in the cross frame. Figure A.7 shows the total stiffener length ($b = b_1 + b_2$) versus the absolute value of average axial force in each angle forming the cross frame. Results are presented for a 60 deg. skew model with L216x216x25.4 mm [L8.50x8.50x1.00 in] angles and a 25.4 mm [1.00 in] stiffener thickness, but were similar for other skew angle, stiffener, and angle combinations.

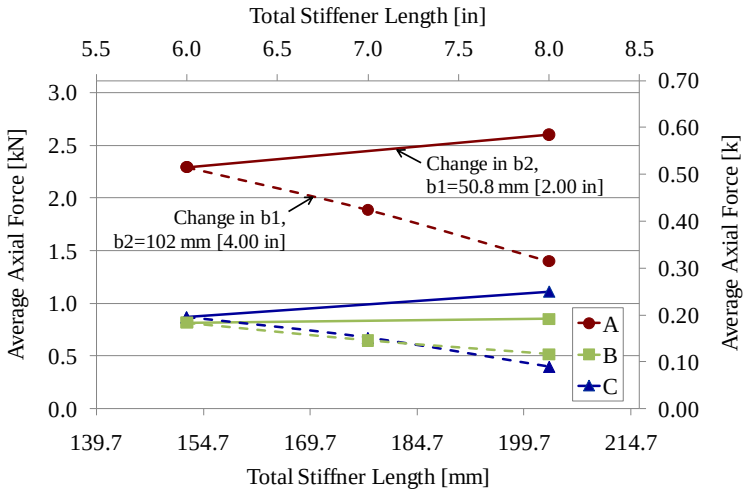

Figure A.7: Effect of increasing stiffener length, 60 deg. skewed bridge with L126x126x25.4 mm [L8.50x8.5x01.00 in] angles and a 25.4 mm [1.00 in] thick stiffener (absolute values shown)

When b_1 was lengthened, the stiffness of the plate decreased as denoted by the broken lines in Figure A.7. In these models, b_2 was held at a constant 102 mm [4.00 in]. Results show the b_1 portion of the stiffener behaves similar to a cantilever with the additional length making it less stiff. Lengthening b_2 increased the stiffness of the assembly, but only slightly, denoted by the

solid lines in Figure A.7. While b_2 was varied, the b_1 dimension was held at 50.8 mm [2.00 in]. The b_2 portion of the stiffener increased the stiffness of the cross frame because it offered additional restraint against bending and slightly reduced unbraced length.

A.4.2: STIFFENER THICKNESS

Increasing stiffener thickness had a much larger effect on the resulting force in the cross frame members than stiffener length. Figure A.8 shows the effect of various stiffener thicknesses in a 40 deg. skewed bridge with L152x152x25.4 mm [L6.00x6.00x1.00 in] angles and a total stiffener length of 152 mm [6.00 in] (b_1 = 50.8 mm [2.00 in] and b_2 = 102 mm [4.00 in]). Results were similar for several other combinations investigated. Figure A.8 shows cross frame stiffness, quantified by axial force in the cross frame, almost doubles when stiffener thickness increases from 12.7 and 19.1 mm [0.500 and 0.750 in] and then increases less significantly between 19.1 and 25.4 mm [0.750 and 1.00 in]. Results illustrate cross frame stiffness theory, showing that the least stiff component (the stiffener or the cross frame member) controlled the stiffness of the cross frame assembly. The stiffness of the cross frame increased significantly between 12.7 and 19.1 mm [0.500 and 0.750 in] because the stiffness of the connection was less than that of the cross frame member. Once the stiffener was thickened, the cross frame member was the least stiff element and increasing stiffener thickness beyond this point did not contribute much to additional cross frame stiffness.

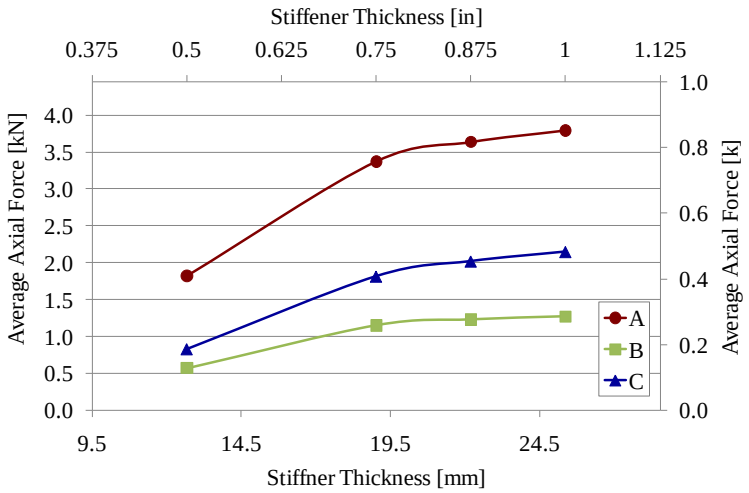

Figure A.8: Effect of increasing stiffener thickness, 40 deg. skewed bridge with L152x152x25.4 mm [L6.00x6.00x1.00 in] angles and a 152 mm [6.00 in] stiffener length (absolute values shown)

A.4.3: CROSS FRAME STIFFENER SELECTION

Stiffener thickness had a larger effect on stiffness of the cross frame assembly than stiffener length. Therefore, a constant bent plate stiffener length of 152 mm [6.00 in] (b_1 = 50.8 mm [2.00 in] and b_2 = 102 mm [4.00 in]) was selected and sub-models were used to select an appropriate stiffener thickness for 10 to 40 deg. skew angles. Average lateral force in each cross frame was compared to that of the non-skewed bridge. Results are presented in Figure A.9. Negative forces represent tension and positive forces represent compression. A solid black line shows force in the non-skewed bridge and black circles denote the selected stiffener thickness.

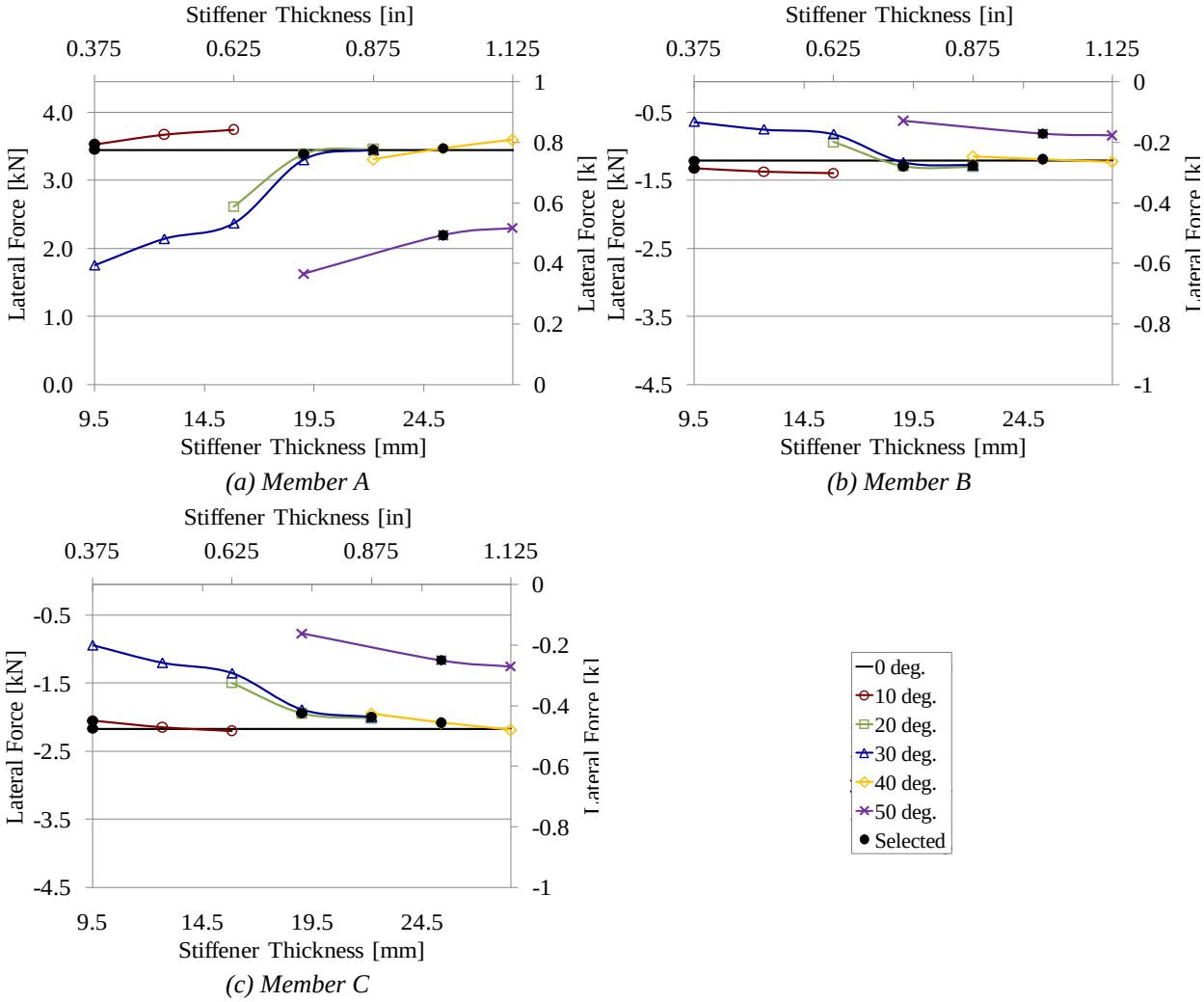

Figure A.9: Stiffener thickness selection

An exception was made for the 40 deg. skew angle, as it was found that stiffener thickness required using the above outlined procedure was over 38.1 mm [1.50 in]. Because this was

considered unrealistic, a larger equal leg angle was selected for the cross frame elements, so a maximum stiffener thickness of 25.4 mm [1.00 in] would be sufficient to match lateral forces produced in the non-skewed bridge. It should be noted that while it is recognized that a 25.4 mm [1.00 in] thick stiffener thickness is also not realistic, the authors found that the stiffener properties drive behavior in bridges with large skew angles.

Selected dimensions for each cross frame assembly are given in Table A.1. Connection stiffeners for the non-skewed bridge were 102 mm [4.00 in] long and 9.53 mm [0.375 in] thick. Dimensions were selected as a practical minimum. Combinations of angle and stiffener determined in the sub-models were then used in the full bridge models for parametric analysis.

Table A.1: Cross frame properties for parametric modeling

Skew Angle deg	*Unbraced Length, L_b mm [in]*	*Angle mm [in]*	*Slenderness Ratio, L_b/r*	*Stiffness, $A\cos^3\theta$ mm^2 [in^2]*	*Connection Stiffener Thickness, t mm [in]*
0	2,832 [111.5]	L108x108x12.7 [L4.25x4.25x0.500]	139.4	2,580 [4.00]	9.53 [0.375]
10	2,979 [117.3]	L114x114x12.7 [L4.50x4.50x0.500]	138.4	2,620 [4.06]	9.53 [0.375]
20	3,122 [122.9]	L121x121x19.1 [L4.75x4.75x0.500]	137.3	2,410 [3.73]	19.1 [0.750]
30	3,388 [133.4]	L133x133x19.1 [L5.25x5.25x0.750]	137.1	3,060 [4.75]	22.2 [0.875]
40	3,830 [150.8]	L152x152x25.4 [L7.00x7.00x1.00]	138.2	2,230 [3.45]	25.4 [1.00]
50	4,564 [179.7]	L152x152x25.4 [L7.00x7.00x1.00]	168.5	1,050 [1.68]	25.4 [1.00]

A.4.4: Effect of Cross Frame Stiffness on Distortion-Induced Fatigue

A separate analysis was conducted using full bridge models before cross frame geometry was finalized to evaluate the effects of cross frame stiffness, specifically varied bent plate stiffener thickness on distortion-induced fatigue, as quantified by HSS. Non-skewed and skewed-parallel bridges with cross frame spaced at 4.57 m [15.0 ft] and 9.14 m [30.0 ft] were investigated with cross frame element (angle) sizes given in Table A.2. Stiffeners in non-skewed bridges were 102 mm [4.00 in] by 9.53 mm [0.375 in] and bent plate stiffeners used in skewed bridges were 152 mm [6.00 in] long and had varied thicknesses.

Table A.2: Cross frame element sizes for evaluating hot spot stresses

Skew Angle, deg.	*Equal Leg Angle, mm [in]*
0	L108x108x12.7 [L4.25x4.25x0.500]
10	L114x114x12.7 [L4.50x4.50x0.500]
20	L121x121x19.1 [L4.75x4.75x0.750]
30	L133x133x19.1 [L5.25x5.25x0.750]
40	L152x152x25.4 [L6.00x6.00x1.00]
50	L178x178x31.8 [L7.00x7.00x1.25]

Results are presented in Figure A.10 and show that cross frame stiffness had a significant impact on HSS#1. HSS#2 was not evaluated in this study. Bent plate thickness affected HSS more significantly than skew angle, although it has not been considered in detail in previous research associated with distortion-induced fatigue. It is also interesting to note that some increases in stiffener thickness changed HSS#1 more significantly than others. This is illustrated well by the 40 deg. skewed-parallel models. The stiffness of the bent plate stiffener limited the stiffness of the cross frame assembly, and HSS increased significantly when thickness was increased from 19.1 to 22.2 mm [0.750 to 0.875 in]. Not much additional stiffness was gained when the stiffener thickness was further increased from 22.2 to 25.4 mm [0.875 to 1.00 in] because it was no longer the most flexible part of the cross frame and connection assembly. No additional HSS would be generated unless the cross frame element was increased in stiffness. Results were similar for bridges with cross frames spaced at 4.57 and 9.14 m [15.0 and 30.0 ft]. HSS magnitudes were higher for the 9.14 m [30.0 ft] cross frame spacing, but relative magnitudes were nearly the same.

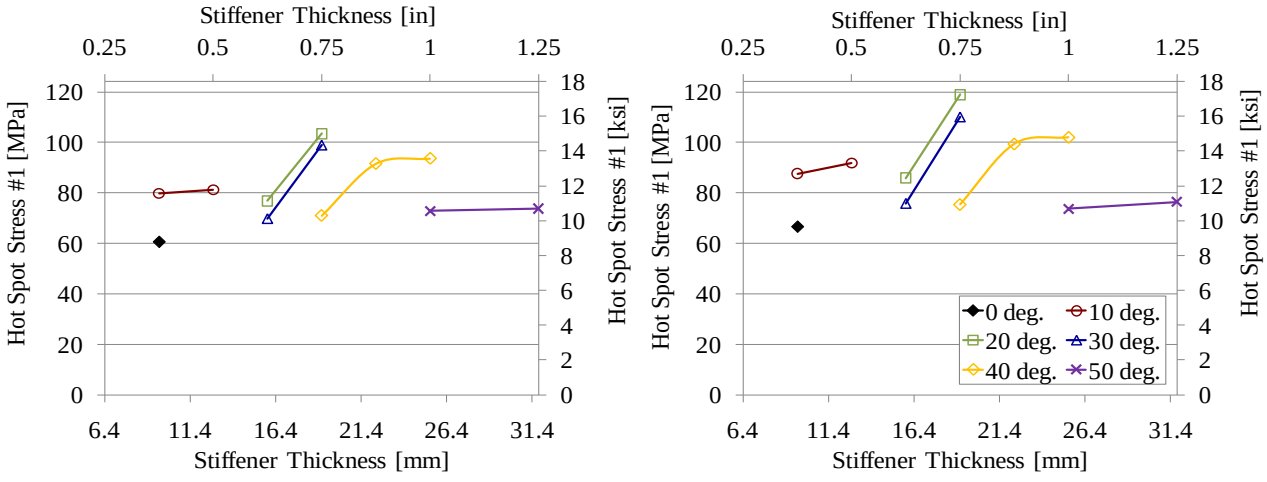

(a) Cross frames spaced at 4.57 m [15.0 ft] *(b) Cross frames spaced at 9.14 m [30.0 ft]*

Figure A.10: Effect of cross frame stiffness on Hot Spot Stress #1

A.5: CONCLUSIONS

Many geometric variations of the bent plate stiffeners were considered to match stiffness of cross frames assemblies with varied skew angle. Cross frame assembly stiffness was quantified by lateral force developed in each cross frame member. As shown in sub-modeling, cross frame stiffness significantly affects the amount of force transferred between girders. Conclusions drawn from these analyses are summarized as follows:

- Cross frame assembly stiffness varies with cross frame element (angle) stiffness and connection stiffness (stiffener). Summing reciprocals of cross frame and connection contributions seems appropriate based on results.
- Skew angle influenced the stiffness of both the cross frame and connection.
- Lengthening the portion of the bent plate stiffener perpendicular to the cross frame decreased the cross frame assembly stiffness, but lengthening the portion parallel to skew increased the cross frame assembly stiffness slightly.
- Increasing stiffener thickness increased cross frame assembly stiffness more significantly than lengthening either portion of the stiffener.
- Cross frame stiffness is an important parameter to consider with respect to distortion-induced fatigue, and was found to have as large of an impact on distortion-induced fatigue stresses as skew angle in skewed-parallel bridge configurations.

Brace stiffness is an important consideration when evaluating distortion-induced fatigue. It has not been explicitly considered in previously conducted studies. This may be one reason that the literature presents conflicting results on some aspects of distortion-induced fatigue, including location of maximum distortion-induced fatigue vulnerability (positive or negative moment region). Cross frame stiffness has a significant effect on load distribution, as well as hot spot stress and distortion-induced fatigue susceptibility. Hot spot stresses are as sensitive to cross frame stiffness as skew angle, cross frame spacing, and bracing configuration. Therefore, cross frame geometry should be selected carefully during design so bracing is adequate, but not so excessively stiff as to increase distortion-induced fatigue vulnerability. Also, implications on cross frame stiffness should be carefully evaluated as repair and retrofit techniques are implemented.

A.6: ADDITIONAL REFERENCES

Yura, J., Phillips, B., Raju, S., and Web, S. (1992). "Bracing of Steel Beams in Bridges." Report No. 1239-4F, Center for Transportation Research, University of Texas at Austin.

APPENDIX B: EFFECT OF WEB GAP LENGTH ON FATIGUE SUSCEPTIBILITY

B.1: PROBLEM STATEMENT

Global parameters including skew angle, cross frame spacing, and bracing configuration were the primary parameters effecting distortion-induced fatigue stresses under investigation. However, distortion-induced fatigue susceptibility is also influenced by localized geometric properties in the web gap such as web gap length, web thickness, brace orientation, and weld configuration. The objective of this secondary investigation was to determine the effect of web gap length on hot spot stresses generated in the web gap region.

B.2: BACKGROUND

Web gap length is defined here as the distance between the end of the connection stiffener and adjacent flange plate as shown in Figure B.1. Connection susceptibility to distortion-induced fatigue cracking is heavily influenced by the length of the weak web gap region over which distortion is absorbed (Fisher et al. 1990). The web gap exists for two purposes: to prevent creation of a fatigue susceptible detail, and to ease construction. If no web gap existed, three welds would intersect where the connection plate, web, and flange meet. The resulting detail could develop a triaxial state of stress and be extremely vulnerable to fatigue and brittle fracture. A detail with no web gap may have problems from lack of fusion or slab inclusions at the weld intersection (Fisher et al. 1990). Also, the presence of a web gap avoids welding in tight corners. At the other extreme, if web gaps become too long, the unstiffened region of the web may be susceptible to web crippling.

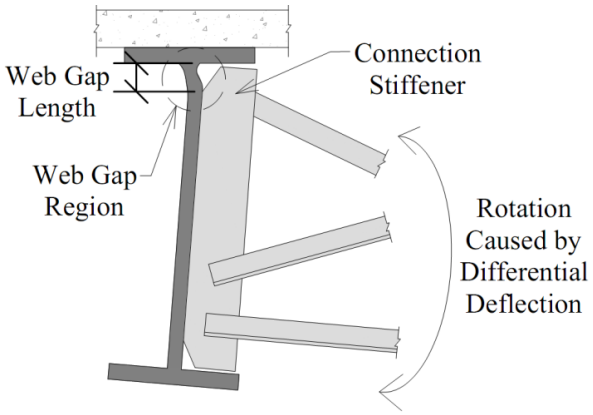

Figure B.1: Web gap length

Web thickness is an important consideration when evaluating web gap length, as a thicker web is less susceptible to local buckling and has more material to resist distortion. Previous researchers have attempted to develop equations predicting web gap stress based on differential deflection. Although no reliable equation has yet been developed, a primary variable in all forms of the expression is the ratio of web gap length to web thickness, g/t_w (Berglund and Schultz 2002). Typical web gap lengths formed by transverse connection stiffeners in bridges range from 38.1 to 76.2 mm [1.50 to 3.00 in] (Fisher et al. 1990). However, this dimension varies widely from state to state. Short web gaps, have less material and length to absorb out-of-plane distortion from differential deflection, highlighted in Figure B.1, therefore are typically considered most susceptible to distortion-induced fatigue (Fisher et al. 1990). Larger web gaps are more flexible allowing them to better accommodate out-of-plane movement and are generally thought of as less susceptible to distortion-induced fatigue.

B.3: MODELING

Bridge geometry was adapted from American Iron and Steel Institute (AISI), Design Example 2 (1997) as this bridge was used for the primary investigation and is described in Section 3.2: Bridge Geometry. A non-skewed bridge configuration was used with X-type cross frames composed of L102x102x15.9 mm [L4.00x4.00x0.625 in] angles spaced at 4.57 m [15.0 ft]. Seven web gap lengths ranging from 25.4 to 152 mm [1.00 to 6.00 in] were investigated; these lengths correspond to dimensions between two and thirteen times the web thickness.

A simplified linear elastic, finite element model was created in Abaqus v6.8-2 (Simulia 2008). Only the differences between the finite element models used to investigate web gap length and those used to study global parameters (skew angle, cross frame spacing, and bracing configuration) are described herein. The majority of modeling information can be found Section 3.3: Finite Element Modeling.

Simplified models contained approximately 810,000 elements and 5.9 million degrees of freedom. S4R shell elements, meshed at 305 mm [12.0 in] were used to model the 203 mm [8.00 in] thick concrete deck. Three-dimensional elements were used for the remainder of the model, including the concrete haunch. No welds were modeled and connections were made using surface-to-surface ties directly between connected parts. Cross frames were meshed at

50.8 mm [2.00 in], which transitioned to a 5.08 mm [0.200 in] mesh near web gap regions. Cross frame members forming an X were not connected in the center with a plate as done in the models used for the primary investigation, to limit bending of the cross frame angles.

A lane load was applied over a 2.13 m [7.00 ft] wide region centered over an interior girder. The 2.13 m [7.00 ft] load width was selected to be twice the deck overhang width, 1.07 m [3.50 ft], so the load could be later applied over an exterior girder if desired. A lane load was used instead of the AASHTO (2007) fatigue truck, because placement to induce maximum stress had not yet been determined by influence surface analysis. The pressure load applied had a magnitude of 10.3 kPa [1.50 psi]. Boundary conditions were modeled using translational restraint applied to the bottom surface of the bottom flange over a 152 mm [6.00 in] wide area center over the point of support. Hot Spot Stresses (HSS) were used to compare distortion-induced fatigue susceptibility in the web gap region as described in Section 3.4: Hot Spot Stress Analysis. Stress concentrations at the intersection of the web and flange (HSS#2) were not quantitatively evaluated during this sub-analysis.

B.4: RESULTS

Maximum HSS developed in the top web gap of the exterior girder adjacent to the loaded interior girder. The most highly stressed web gap was in the positive moment region for all web gap sizes considered. Stress magnitude is plotted in Figure B.2 for each web gap length. Web thickness in the positive moment region was 11.1 mm [0.4375 in].

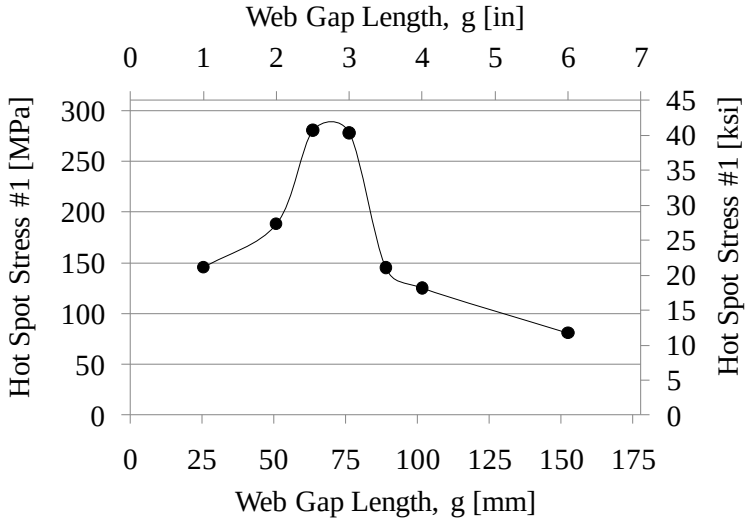

Figure B.2: HSS #1 for varied web gap lengths

Web gap stress varied significantly over the range of web gap lengths evaluated, confirming the significant impact of local geometric characteristics. Stress magnitudes generated in the finite element model with a 63.5 mm [2.50 in] web gap were approximately four times higher than those generated in the model with a 152.4 mm [6.00 in] web gap. Figure B.2 shows that the highest stresses developed in models with web gap lengths towards the middle of the range considered, rather than in the shortest web gaps. It was found that short web gaps are sufficiently restrained by connected elements to prevent development of the largest web gap stress magnitudes. As noted in previous research, long web gaps, which are more flexible, have additional length to accommodate out-of-plane distortion caused by rotation and do not develop the highest web gap stresses. Maximum hot spot stress occurred for web gap lengths of 63.5 and 76.2 mm [2.50 and 3.00 in], which are both on the long end of the range of web gap lengths used in practice reported by Fisher et al. (1990). Peak stresses found in this study occur between five and seven times the web thickness. Limitations of the linear elastic finite element model used should be noted, as local web buckling and yield were not considered. A 25.4 mm [1.00 in] web gap length was selected for use in the primary investigation, which is approximately two times the web thickness.

B.5: CONCLUSIONS

Concentrated stress generated in web gap regions was found to vary significantly based on web gap length; this agrees with prior research which has concluded that distortion-induced fatigue susceptibility is not only related to global parameters, but also highly sensitive to local geometry (Fisher et al. 1980, Fisher et al. 1990, Berglund and Schultz 2002, and Li and Schultz 2005). Stress magnitudes developed in short web gaps were higher than those developed in long web gaps, but web gap lengths in the middle of the range considered produced the highest stress magnitudes. By avoiding short web gaps (less than 50.8 mm [2.00 in]) and very long web gaps (more than 102 mm [4.00 in]), bridges may have been inadvertently designed with web gap lengths that optimize risk of distortion-induced fatigue. As state DOTs work to retrofit bridges for distortion-induced fatigue, localized web gap geometry should be considered in addition to global parameters, including both web gap length and web thickness. Lengthening short web gaps using techniques such as slotting the connection stiffener may produce undesirable results if final web gap length is not carefully chosen.

B.6: ADDITIONAL REFERENCES

Berglund, E. and Schultz, A. E. (2002). "Analysis Tools and Rapid Screening Data for Distortional Fatigue in Steel Bridge Girders." *Final Report 2002-06*, Minnesota Department of Transportation, St. Paul, MN.

APPENDIX C: INFLUENCE SURFACES RELATING LOAD PLACEMENT AND WEB GAP STRESSES

C.1: PROBLEM STATEMENT

Fatigue in steel bridges results from cyclic traffic loading. AASHTO (2007) fatigue loading consists of a fatigue truck placed to induce maximum demand, but the definition of demand with respect to distortion-induced fatigue is not well-defined. Differential deflection has been used in previous research to determine relative distortion-induced fatigue susceptibility of a bridge system (Berglund and Schultz 2006, Tedesco et al. 1995, and Cousins and Stallings 1998). However, because fatigue and fracture are driven by cyclic stresses, stresses in the web gap region may be a more accurate measuring stick. Additionally, prior research has demonstrated that the location of maximum differential deflection does not always correspond to the location of maximum Hot Spot Stress (HSS) (Hartman et al. 2010). Fatigue truck placement to induce maximum distortion-induced fatigue-related stresses is not obvious from previous research. Therefore, varied unit load placements were used to develop influence surfaces for three bridge configurations relating location and magnitude of distortion-induced fatigue-related stress to load placement. Results from influence surface analysis were then used to determine truck placement for all bridge configurations investigated.

The primary objective of this portion of the overall study was to determine critical live load placement on the bridge deck to induce maximum distortion-induced fatigue-related HSS for each bridge configuration considered in the parametric analysis, and gain a better understanding of the relationship between load placement and web gap stresses. Secondary objectives were to identify regions of the bridge most susceptible to distortion-induced fatigue, determine corresponding load placements, and to compare bridge response for each configuration, including critical load placement and regions of highest susceptibility.

C.2: MODELING METHODOLOGY

C.2.1: BRIDGE GEOMETRY

Bridge geometry was adapted from American Iron and Steel Institute (AISI), Design Example 2 (1997) and was essentially the same as that used for parametric analysis. Details concerning bridge geometry and finite element modeling can be found in Sections 3.2 and 3.3 respectively

with only differences described herein. Influence surfaces were created for the non-skewed, 40 deg. skewed-parallel, and 40 deg. skewed-staggered bridge configurations (Figure 1). Cross frame spacing was 4.57 m [15.0 ft] for all three configurations.

Cross frames placed parallel to skew angle in the skewed-parallel and skewed-staggered bridges consisted of L152x152x25.4 mm [L6.00x6.00x1.00 in] angles with a 22.2 mm [0.875 in] thick bent connection stiffener (Figure 3). Influence surface analysis was conducted before cross frame geometry refinements for stiffness was completed and therefore has a smaller cross frame angle/stiffener combination than the 40 deg. skewed bridges used in parametric models. Models with finalized cross frame geometry were spot checked against models used to generate influence surfaces. Differences in the skewed-staggered configuration were negligible because the location of maximum stress occurred in the positive moment region where non-skewed cross frames were used. Two differences were noted in the skewed-parallel configurations. First, the HSS#1 path was 0.752 mm [0.030 in] closer to the weld toe than in the non-skewed bridge due to increased stiffener thickness, which resulted in different relative node location with respect to the stiffener to web weld. Maximum stress magnitudes resulting from five critical unit load placements over an interior girder were compared and showed, because stresses were determined closer to the weld toe, HSS#1 magnitudes were approximately 8.85% higher than they would have been if stresses had been pulled 5.08 mm [0.200 in] from the weld toe as was done for non-skewed cross frames. Secondly, use of a less stiff cross frame (angle/stiffener assembly) resulted in approximately 6.15% lower HSS on average than would have been generated if the finalized cross frame geometry was used. This was determined by comparing bridge models with different cross frames subjected to truck loading. Results of detailed comparisons showed the differences approximately offset each other and no modification was required.

C.2.2: LOADING

Unit loads were strategically placed throughout the bridge deck to develop influence surfaces. A 0.305 m [1.00 ft] by 0.305 m [1.00 ft] grid was established on each bridge deck. Accordingly, a 4.45 kN [1.00 kip] load was applied as a pressure load acting over a 645 mm^2 [1.00 ft^2] area. Load placements considered for each influence surface and grid systems are shown in Figure C.1. Symmetry was used when possible to reduce the number of loaded surfaces necessary to generate an accurate influence surface.

The non-skewed bridge was treated as a doubly symmetric bridge and was divided into four quadrants for loading as shown in Figure C.1a. This idealization was not entirely accurate due to lack of symmetry in cross frames, but was considered a reasonable assumption and verified by placing a few loads in the remaining quadrants. A total of 400 load placements were considered with a majority of loads placed on the west half of the bridge and slightly more loads placed on the northwest quadrant than the southwest quadrant. The assumption of double symmetry was verified as reasonable, therefore all stress envelopes show results mirrored from the northwest quadrant to maintain a high level of detail. Because influence surface contours produced in the non-skewed bridge were smooth, less load cases were deemed necessary in future influence surface analyses.

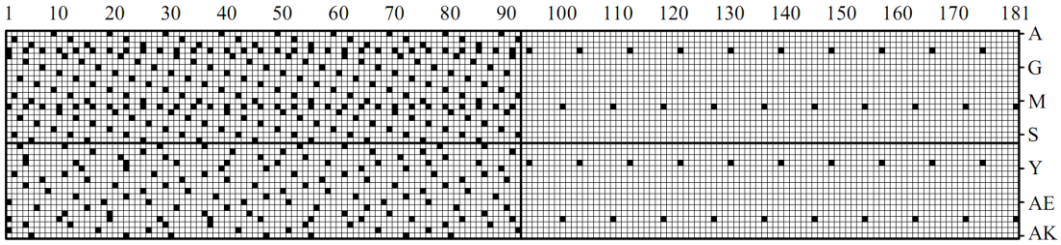

(a) Non-skewed bridge, 400 loaded surfaces

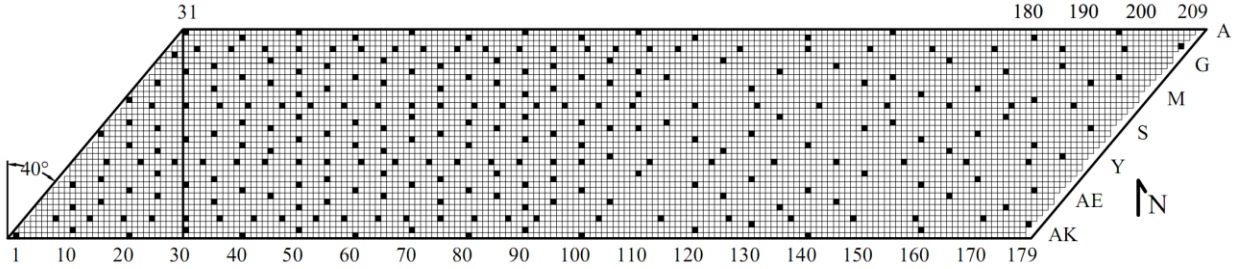

(b) 40 deg. skewed-parallel bridge, 258 loaded surfaces

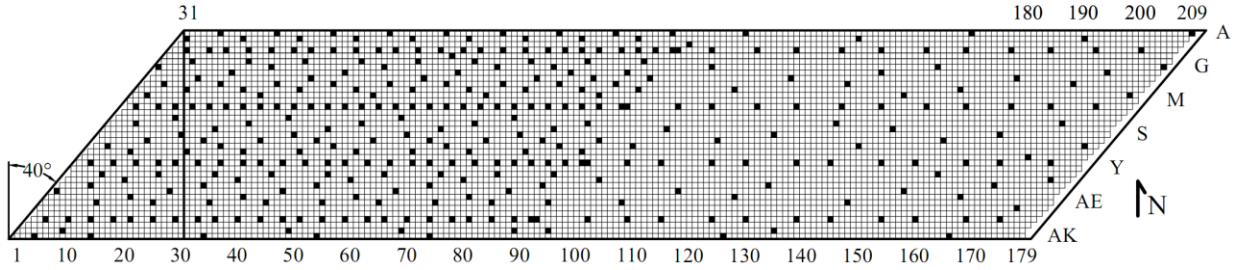

(c) 40 deg. skewed-staggered bridge, 350 loaded surfaces

Figure C.1: Bridge deck grid for loading and load placements analyzed

Skewed bridges were idealized as singly symmetric for load placement, having two skewed halves corresponding to the two spans, again with verification conducted by placing a few loads on the opposite span. Load locations were concentrated on the west side of the bridge. A total

of 258 load placements were considered for skewed-parallel bridges (Figure C.1b) and 350 load placements were considered for skewed-staggered bridges (Figure C.1c).

C.2.3: Hot Spot Stress

Hot spot stresses (HSSs) were used to compare fatigue susceptibility. Two HSS paths were used to quantify the stress concentration at the connection plate to web weld (HSS#1) and the flange to web weld (HSS#2). Stress magnitudes were determined for both stress paths in each web gap (top and bottom) on both sides of the web (north and south). Data collection and stress paths are described in detail in Section 3.4.

C.3: Refined Boundary Conditions

C.3.1: Purpose

High stress concentrations were found to occur in web gap regions at supports where boundary conditions were applied. It was unclear if these stress concentrations resulted from distortion-induced fatigue or were artificially induced by approximated modeling techniques and proximity to boundary conditions. Additional finite element models with refined boundary conditions were created for comparison. Refined boundary conditions were not implemented in all models due to time constraints and additional computation required.

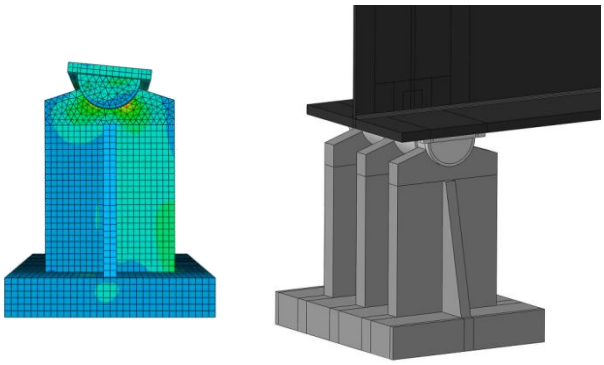

Figure C.2: Refined boundary conditions

C.3.2: Modeling

Refined pin and roller supports were modeled based on the typical geometry presented in the KDOT (2010) bridge design manual and are similar to those used by many state DOTs. Refined supports consisted of two parts as shown in Figure C.2. The top portion was rigidly connected to the bottom flange using tie constraints. Interaction between parts included friction (μ = 0.35)

and hard contact. Translational restraint was then applied to the bottom surface making the bearing a pin or a roller, as appropriate. Bearings were modeled with the same steel material properties used throughout the bridge. Linear-elastic C3D8R brick elements, meshed at 12.7 mm [0.500 in] were used along with C3D6 wedge elements in regions with curved geometry.

C.3.3: RESULTS

Two, four, and five load placements with refined boundary conditions were considered for the non-skewed, skewed-parallel, and skewed-staggered bridges respectively. Load placements were chosen to maximize stress at supports so load placements on the deck overhang and over an interior girder in the positive moment region were considered. Results were similar for the all three bridge configurations. Comparisons of boundary conditions with the same load placement show artificially high stress concentrations in the bottom web gap at both abutments as well as over the pier and in the top web gap at both abutments due to the approximated boundary conditions. Graphical results are presented in Figure C.3 for the non-skewed bridge model that generated maximum stress at supports (surface A39, Figure C.1). Modeling techniques increased stress at both cross frame to web (HSS#1) and web to flange (HSS#2) welds.

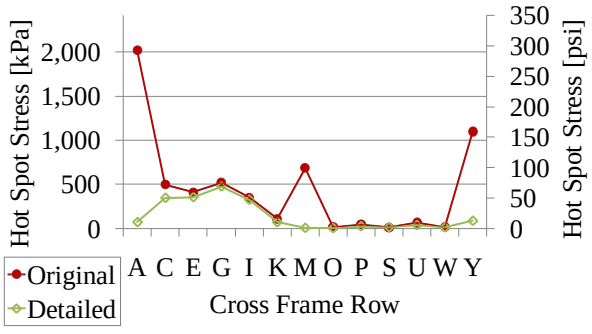

(a) Girder 2, bottom south web gap, HSS#1

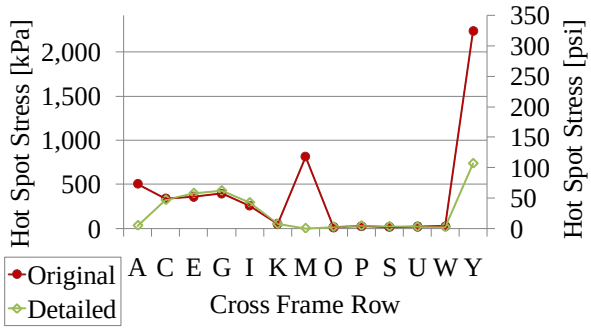

(b) Girder 2, bottom south web gap, HSS#2

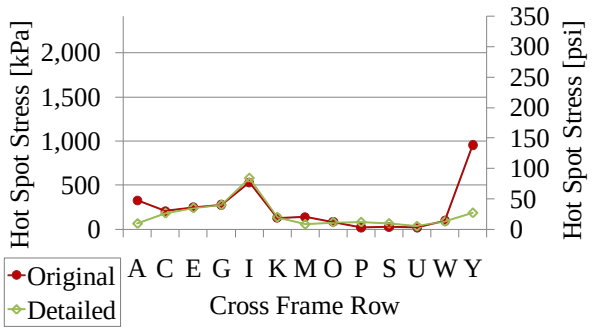

(c) Girder 2, top south web gap, HSS#1

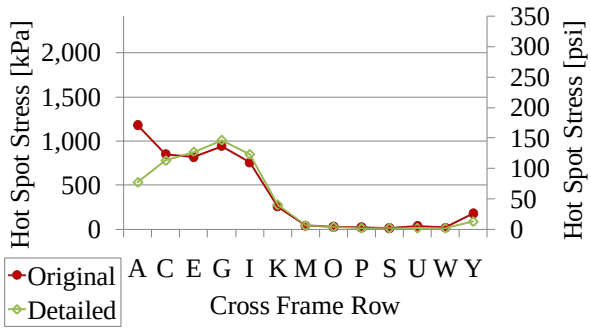

(d) Girder 2, top south web gap, HSS#2

Figure C.3: Comparison of stresses due to boundary conditions (non-skewed bridge with unit load at A39)

Stress concentrations were found to still exist in web gaps at supports in models with refined boundary conditions, although magnitudes were significantly lower. In addition, actual stress magnitudes at supports were found to be lower than stress concentrations developed in positive moment regions by a minimum of 16% for all load placements evaluated, and were not critical for this investigation.

After several bridge models with refined boundary conditions were analyzed, it was determined that stress concentrations occurring at cross frames over the abutments and pier could be safely neglected. Therefore, stress magnitudes generated in these web gaps were taken as zero for the remainder of the influence surface analysis, although small concentrations did occur.

C.4: RESULTS

C.4.1: MULTIPLE STRESS CONCENTRATION TYPES

Two separate stress concentration occurred in all bridge models as expected, confirming experimental observations by Fisher et al. (1990). A stress concentration between the connection plate and web (HSS#1) always occurred on the opposite side of the web as the stress concentration between the flange and web (HSS#2) due to reverse curvature bending in the web gap as shown in Figure C.4. Magnitudes of both stress concentrations were determined for every bridge as described in Section 3.4. The directional stresses (x, y, and z) were compared for both types of stress concentrations and the primary directional contributors are described in Appendix D: A Detailed Look at Web Gap Stresses.

HSS#2 was only found to be significant in the top web gap and did not produce high stress magnitudes in the bottom web gap for any bridge configuration. The bridge deck restrains rotation of the girder top flange, therefore causing a high stress concentration when the cross frame pulls on the web. The bottom flange tends to be much more flexible and can move to maintain an angle closer to 90 deg. with the beam web. Therefore, in web gaps adjacent to the bottom flange, cross frame movement causes the bottom flange to rotate, but prevents the development of a second stress concentration.

Depending on the details used, HSS#2 may be reduced or prevented by use of tight fit or positively attached connection stiffeners. If the angle between the flange and web is held near 90 deg. by stiffeners (connection, transverse, and/or bearing) HSS#2 may be prevented, because the

flange is engaged through bearing on the stiffener. The geometry used has a 1.27 mm [0.0500 in] gap between the end of the connection plate and the flange, therefore some flange rotation occurred. HSS#1 was considered separately from HSS#2 because the importance of each may be heavily based on the individual bridge geometry and weld quality.

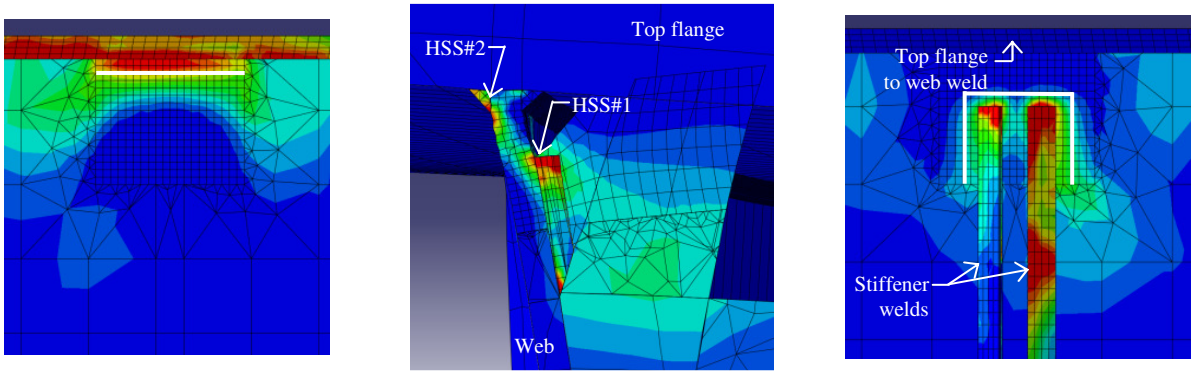

(a) HSS#2: Side of web opposite the stiffener with top flange removed

(b) End view showing stress distribution

(c) HSS#1: Connection stiffener and top flange have been removed

Figure C.4: Stress concentrations

C.4.2: NON-SKEWED BRIDGE

Results from the non-skewed bridge are primarily described in Section 4. Additional influence surfaces for the row of cross frames with the highest HSS, cross frame row G, are shown in Figure C.5 and Figure C.6. Influence surfaces were numbered using the girder number (G1), cross frame row (G), web gap location, side of web (top or bottom and north or south, TN), and HSS path (1 or 2). Only the west span of the bridge is shown. The cross frame to web intersection containing the web gap of interest is also circled in the figure.

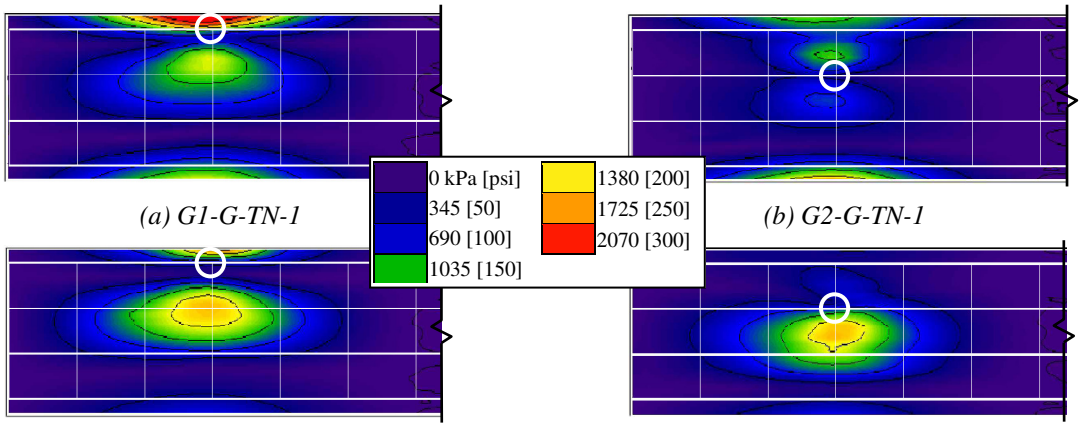

(a) G1-G-TN-1

(b) G2-G-TN-1

(c) G1-G-TS-1

(d) G2-G-TS-1

Figure C.5: HSS#1 influence surfaces of the non-skewed bridge for the top web gap in cross frame row G on the (a) exterior side of the north (top) exterior girder, (b) interior side of the exterior girder, (c) exterior side of the interior girder, and (d) interior side of the north interior girder

Maximum HSS#1 excluding loads placed on the deck overhang were caused by loads placed near an interior girder (Figure C.5c) and loads centered on the bridge (Figure C.5d). Maximum HSS#2 also occurred due to the same two load placement, but occurred in different web gaps (Figure C.6a and b).

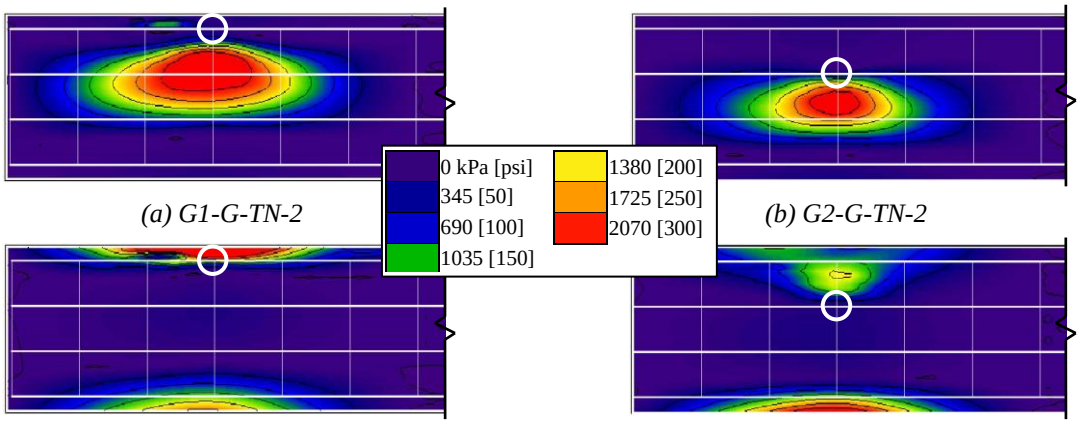

(a) G1-G-TN-2 *(b) G2-G-TN-2*

(c) G1-G-TS-2 *(d) G2-G-TS-2*

Figure C.6: HSS#2 influence surfaces of the non-skewed bridge for the top web gap in cross frame row G on the (a) exterior side of the north (top) exterior girder, (b) interior side of the exterior girder, (c) exterior side of the interior girder, and (d) interior side of the north interior girder

C.4.3: 40 DEG. SKEWED-PARALLEL BRIDGE

Envelope surfaces were developed for both HSS#1 and HSS#2 and are shown in Figure C.7. HSS#1 magnitudes were much higher than in the non-skewed bridge and HSS#2 magnitudes were slightly lower. HSS#1 and HSS#2 were very similar in magnitude.

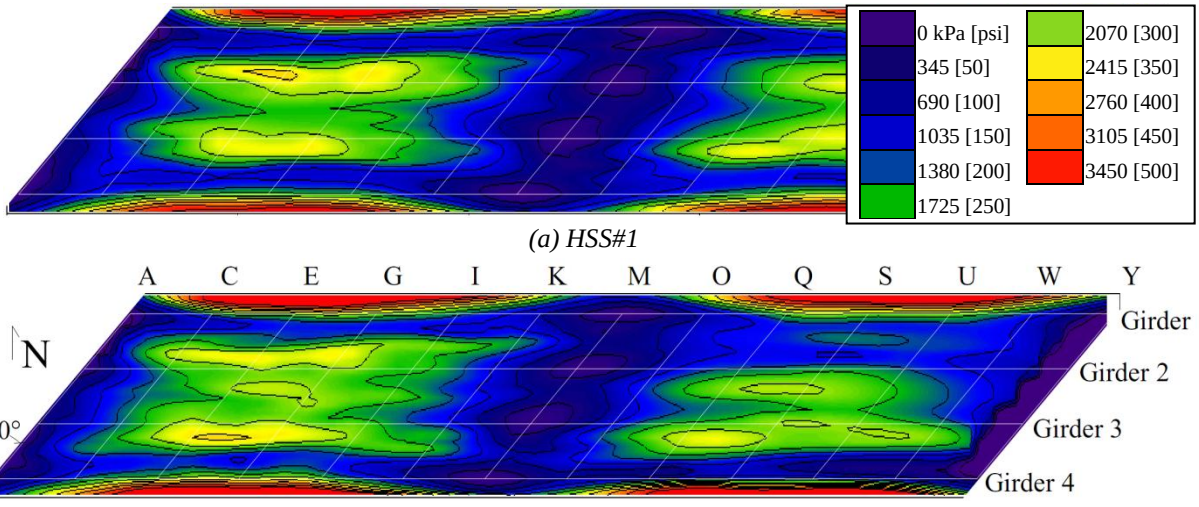

(a) HSS#1

(b) HSS#2

Figure C.7: Envelope surfaces for the skewed-parallel bridge

Influence surfaces are presented in Figure C.8 for web gaps which had the highest HSS#1 and HSS#2 magnitudes, for load placement outside of the deck overhang. Maximum HSS#1 occurred in the top web gap on the interior side of the exterior girder and resulted from loads placed over an interior girder in the positive moment region. Maximum stress magnitude was approximately 30% (6895 kPa [100 psi]) higher than the same load placement and stress concentration in the non-skewed bridge. Results for HSS#1 agree with previous research predicting that distortion-induced fatigue susceptibility increases with skew angle (Fisher and Mertz 1984; Berglund and Schultz 2006). Maximum HSS#2 decreased approximately 10% (345 kPa [50 psi]) from the non-skewed bridge, but occurred in the same location and resulted from the same load placement. Maximum HSS#2 occurred in the top web gap on the exterior side of the exterior girder and was caused by loads placed near the interior girder.

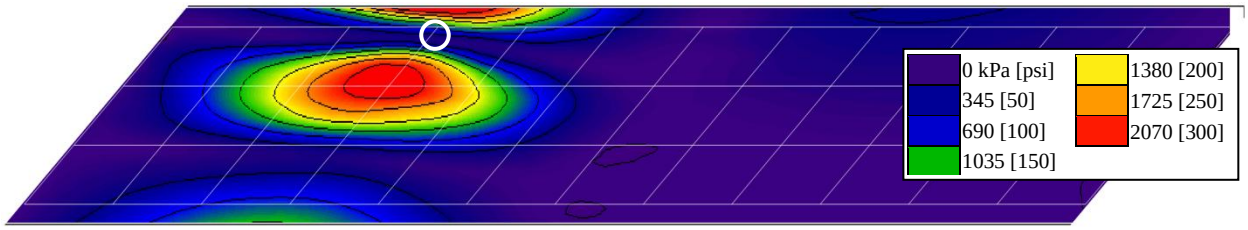

(a) G1-G-TS-1

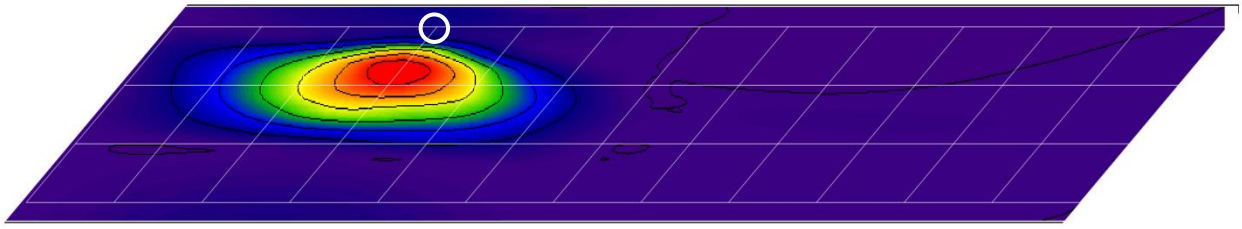

(b) G1-G-TN-2

Figure C.8:Influence surfaces for 40 deg. skewed-parallel bridge showing the top web gap of cross frame row G on the (a) interior side of the north (top) exterior girder showing HSS#1, and (b) exterior side of the north exterior girder

C.4.4: 40 DEG. SKEWED BRIDGE WITH STAGGERED CROSS FRAMES

Envelope surfaces for the 40 deg. skewed-staggered bridge are presented in Figure C.9. Maximum HSS#1 magnitudes were between those found in the non-skewed and skewed-parallel bridge configurations and occurred in the bottom web gap. HSS#2 was significantly lower that magnitudes in the other two bridge configurations. Figure C.9 also illustrates that loading in the northwest corner of the bridge, the obtuse corner, produced slightly larger HSS#1 and HSS#2 magnitudes that loads placed in the southwest (acute) corner.

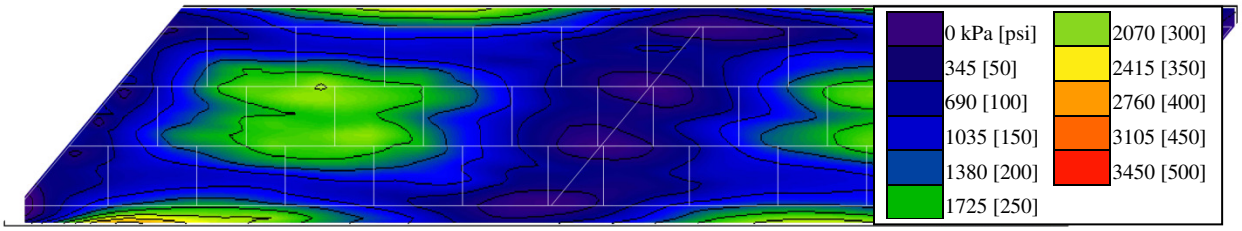

(a) HSS#1

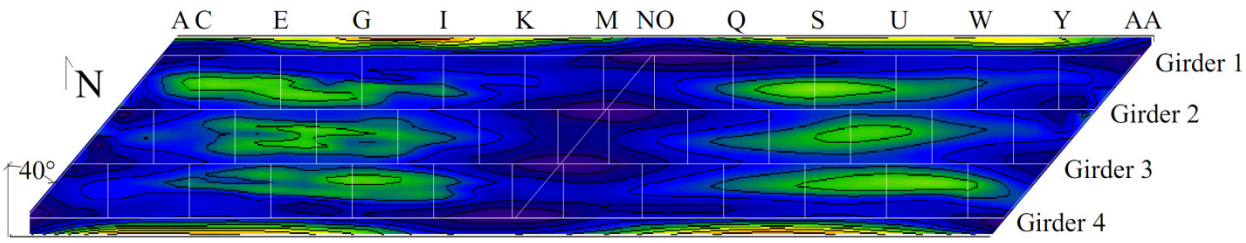

(b) HSS#2

Figure C.9: Envelope surfaces for the skewed-staggered bridge

High magnitudes of HSS#1 in the bottom web gap are likely due to bottom flange out-of-plane movement, which is restrained in cross frame configurations with cross frames placed back-to-back. Figure C.10 illustrates the difference in out-of-plane (transverse or perpendicular to the girder line) between similar load placement on the non-skewed (Figure C.10a) and 40 deg. skewed-staggered bridges (Figure C.10b). Cross frame row E is shown along with Girder 1 (left) and Girder 2 (right). The deflection is magnified 5,000 times in both images and the deflection contours are the same and range from 0.0025 (blue) to 0.0150 mm (red) [0.0001 to 0.0006 in]. Although displacements are small, they are proportional to the total load magnitude placed on the bridge of 4.45 kN [1.00 k].

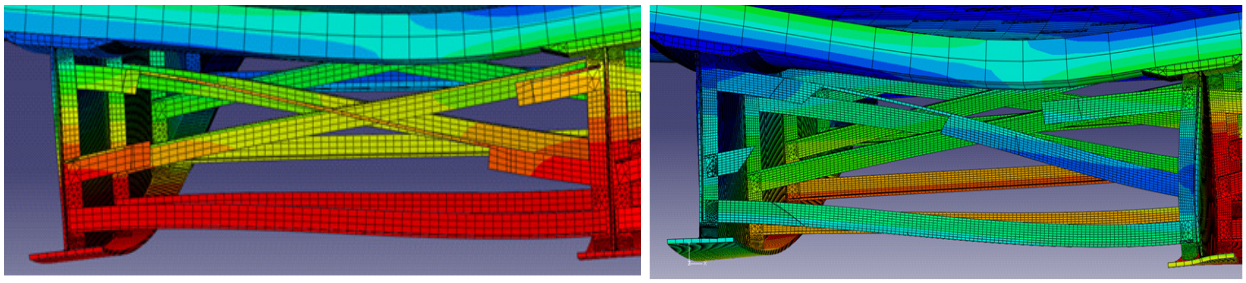

(a) Non-skewed bridge, load placement L32 *(b) Skewed-staggered bridge, load placement K51*

Figure C.10: Comparison of out-of-plane movement at cross frame row E, magnified 5,000 times contoured between 0.0025 (blue) to 0.0150 mm (red) [0.0001 to 0.0006 in]

Contours in the deck are nearly identical, but displacement contours near the bottom flange are very different. The bottom flanges in the non-skewed bridge move together and the cross frame

between Girder 1 and Girder 2 (left) and Girder 2 and Girder 3 (right) are also contoured evenly. In the skewed-staggered bridge, the bottom flanges are at slightly different positions, but more importantly the cross frames on either side of Girder 2 are completely different colors, showing that Girder 2 was forced into reverse curvature out-of-plane along the length of the girder due to the skewed-staggered cross frame configuration.

C.4.4: TABULAR RESULTS

Tabular results are presented in Table C.1 for each bridge configuration considering all load placements except those placed on the deck overhangs. The stress magnitude, web gap ID, and unit load placement are presented for both stress types. Figure C.1 shows the discrete bridge decks with labeled grids used for loading. Note that a representative sampling of possible unit load placements were modeled, so values presented herein may not represent the absolute maximum stress magnitude possible. Tabular values can be used to draw similar conclusions as influence surfaces.

Table C.1: Maximum stress magnitudes excluding loads placed on the deck overhang

Bridge configuration		Non-skewed	40 deg. skewed-parallel	40 deg. skewed-staggered
HSS#1	Stress, kPa [psi]	1,700 [247]	2,450 [355]	2,060 [299]
	Web gap ID	G3-D-TN	G1-C-TS	G2-D1-BS
	Load location	T45	L51	N53
HSS#2	Stress, kPa [psi]	2,730 [396]	2,450 [355]	1,930 [280]
	Web gap ID	G1-C-TN	G1-C-TS	G1-C1-TN
	Load location	L32	D62	K51

Loads placed on the bridge deck overhang induced maximum stress in all three bridge configurations, although as previously discussed, high cyclic loading is not likely in this region. HSS#2 was higher than HSS#1 for this load placement. Table C.2 shows the maximum stress magnitude, corresponding web gap ID, and load location for all load placements in each bridge configuration. The skewed-parallel bridge produced the highest stress followed closely by the non-skewed bridge. Stress generated in the skewed-staggered bridge was much lower than that produced in the other two bridge configurations.

Table C.2: Maximum stress magnitudes

Bridge configuration		Non-skewed	40 deg. skewed-parallel	40 deg. skewed-staggered
HSS#2	Stress, kPa [psi]	4,410 [639]	4,630 [672]	3,070 [445]
	Web gap ID	G4-D-TN	G4-D-TN	G4-E1-TS
	Load location	AK47	AK71	A77

C.5: CONCLUSIONS

The influence surface analysis described herein used over 1,000 detailed, solid element, three-dimensional finite element models to determine the relationship between load placement and web gap stress for a non-skewed, 40 deg. skewed-parallel, and 40 deg. skewed staggered bridge configuration. Both location and magnitude of maximum web gap stresses were considered. Results of the study are summarized below:

- Stress concentrations were found to occur at both the web to connection plate weld (HSS#1) and web to flange weld (HSS#2). Maximum magnitudes occurred in different web gaps and resulted from different load placements, but both are important considerations when evaluating susceptibility to distortion-induced fatigue.
- Loads placed in the positive moment region near interior girders caused the highest distortion-induced fatigue-related stresses when loads placed on the deck overhang were excluded.
- Maximum HSS#1 magnitudes occurred in top web gaps on the interior side of the exterior girders in the positive moment region for the non-skewed and skewed-parallel bridge configurations, and in the bottom web gaps of the interior girder in the positive moment region for the skewed-staggered bridge.
- Maximum HSS#2 magnitudes occurred in the top web gaps in the positive moment region for all three bridge configurations.
- HSS#2 magnitudes were about 35% higher than HSS#1 magnitudes for the non-skewed bridge, approximately the same for the skewed-parallel bridge, and around 6% lower than HSS#1 magnitudes for the skewed-staggered bridge.
- Stress magnitudes were slightly (around 5%) higher for loads placed over an interior girder in the obtuse corner than those placed over an interior girder in the acute corner for skewed-staggered bridges.
- Both load placement within the span and relative to individual cross frames and girders must be considered when analyzing the relationship between load placement and web gap stress.

Previous research has determined load placement to maximize differential deflection, but little prior work has been done to evaluate effects of load placement on web gap stresses directly.

Understanding how load placement effects the location and magnitude of maximum HSS is the first step to determining how and where corrective and/or preventative measures should be taken to extend the life bridges susceptible to distortion-induced fatigue.

C.6: ADDITIONAL REFERENCES

Cousins, T.E. and Stallings, J.M. (1998). "Laboratory Tests of Bolted Diaphragm-Girder Connections." *Journal of Bridge Engineering*, 3(2), 56-63.

Tedesco, J.W.; Stallings, J. M.; and Tow, D.R. (1995). "Finite Element Method Analysis of Bridge Girder-Diaphragm Interaction." *Computers and Structures*, 56(2-3), 461-473.

APPENDIX D: A DETAILED LOOK AT WEB GAP STRESSES

D.1: PROBLEM STATEMENT

Differential deflection and subsequent cross frame rotation produces an extremely complex, three-dimensional state of stress in the web gap region, which is the measure used in the primary investigation to determine relative distortion-induced fatigue susceptibility. Although maximum principal stress was used to quantify results in this investigation, it is important to have an understanding of stresses in each direction in order to compare finite-element results to experimental results and those presented in previous research. Stresses in the web gap region at both the web to connection plate and web to flange weld are evaluated here based on directional and three-dimensional states of stress in non-skewed and skewed bridges to better understand the complex stress state and relative magnitudes of directional stresses.

D.2: MODELING

Web gap stresses were analyzed in bridge models constructed for the primary investigation using Hot Spot Stress (HSS) analysis. Bridge geometry and modeling techniques are described in Section 3.2: Bridge Geometry and Section 3.3: Finite Element Modeling respectively. All bridges included in this evaluation have cross frames spaced at 4.57 m [15.0 ft]. Directional stresses were evaluated in the non-skewed bridge created to develop an influence surface. Loading consisted of a 4.45 kN [1.00 k] load placed near an interior girder in the positive moment region (at L32 on the established deck grid shown in Figure C.1). Load placement considered produced maximum web gap stress magnitude excluding loads placed on the deck overhang. Effects of skew angle on web gap stress were evaluated using fatigue truck loading on skewed-parallel models used for parametric analysis.

D.3: RESULTS

In all models, maximum web gap stress occurred in the top web gap of the exterior girder at cross frame row G, which is located in the positive moment region (refer to Figure 1). Therefore, all results presented are taken from either side of the web at this web gap location. Cross frame rotation caused the web gap to deform in double curvature, creating tensile principal stress concentrations at the web to connection stiffener weld on the interior side of the exterior girder (HSS#1) and at the web to flange weld on the exterior side of the exterior girder (HSS#2).

D.3.1: DIRECTIONAL STRESSES

An overview of the model used to evaluate relative magnitudes of directional stresses is presented in Figure D.1 and shows a section cut at cross frame row G. Directional stresses as well as maximum principal stresses generated in the web gap being analyzed are presented in Table D.1. The connection stiffener has been removed in screen shots of the interior side of the girder for clarity and only the welds remain. All stress contours were set at equal values and range from 0.00 to 3.45 MPa [0.500 ksi] with red being the highest stress values and blue being the lowest. Although stresses are small, they are proportional to the total load magnitude placed on the bridge of 4.45 kN [1.00 k]. Deflections shown in both figures have been magnified 5,000 times so they can be more easily seen.

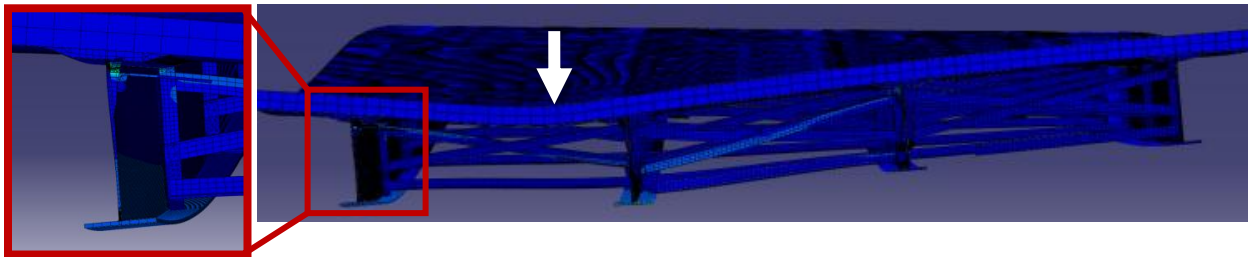

Figure D.1: Overview of web gap location

HSS#2 was found to be driven primarily by vertical, in-plane stress. Relative rotation between the top flange and web creates high tensile stresses on the side of the web that forms an obtuse angle with the top flange. Load placement on the deck causes the top flange to rotate slightly and cross frame rotation pulls the web in the opposite direction.

Hot spot stress magnitudes at the web to flange weld (HSS#2) were much higher than those at the connection stiffener to web weld (HSS#1). This was also noted in an experimental study by Fisher et al. (1990). However, the web to flange weld is typically smooth and of higher quality than the connection stiffener to web weld, therefore distortion-induced fatigue cracking more frequently occurs at the connection stiffener to web weld.

All three-directional stresses contribute to the HSS#1 stress concentration on the interior side of the girder. Longitudinal, in-plane stress had the highest magnitude and largest size with vertical, in-plane stress slightly smaller. Out-of-plane stress does not cover a very big area, barely extending outside of the welds. However, the localized out-of-plane stress concentration penetrates further into the weld than either in-plane stress.

Table D.1: Directional stresses

	End View	*Exterior Side (HSS#2)*	*Interior Side (HSS#1)*
Maximum Principal	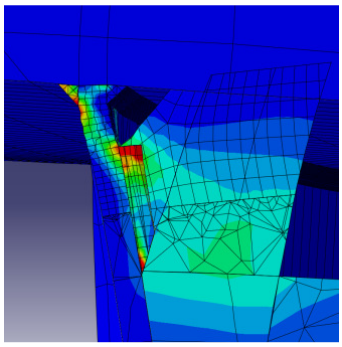	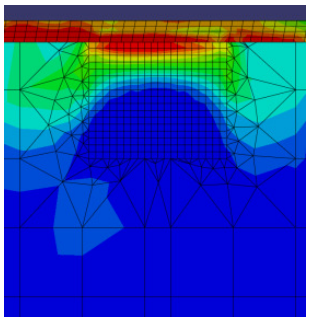	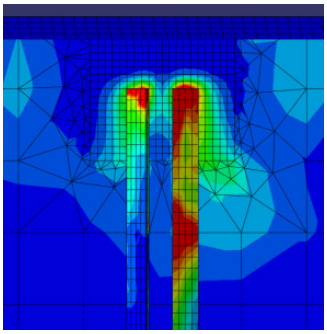
Out-of-Plane	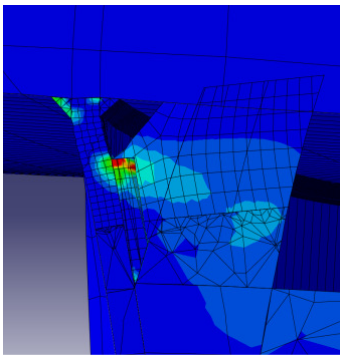	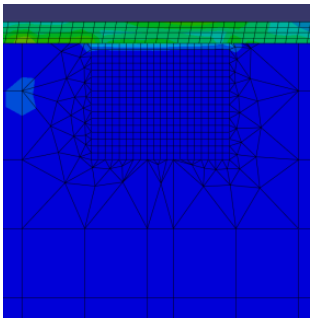	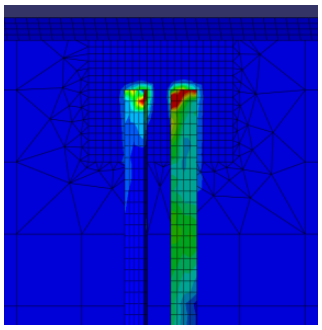
Vertical, In-Plane	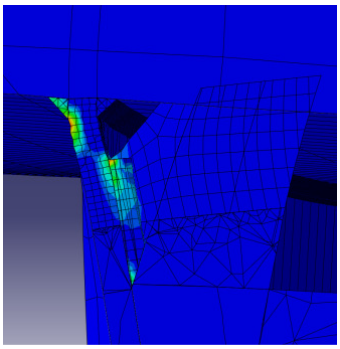	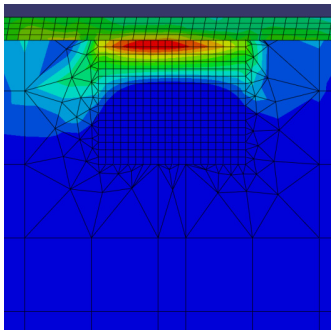	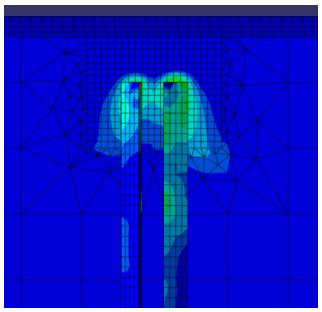
Longitudinal, In-Plane	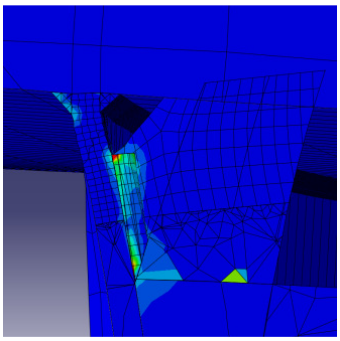	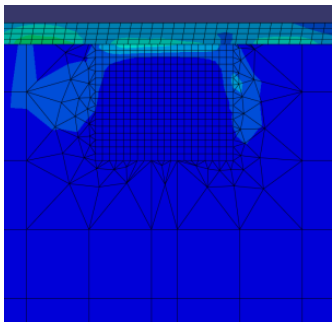	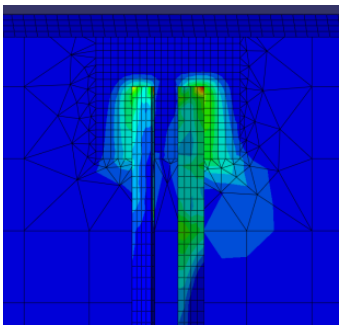

D.3.2: Effect of Skew on Web Gap Stresses

Maximum principal web gap stresses are shown in Figure D.2 for each skew angle modeled in skewed-parallel bridge configurations. All three directional stresses were evaluated, and changes due to skew angle were similar to those observed for maximum principal stress. The connection

plate and welds have been removed for clarity and figures show the interior side of the exterior girder. Stress contours are equal in all figures and range from 0 to 172 MPa [25.0 ksi]. The densely meshed web gap region widens with skew angle as the connection stiffener thickness used increased. Accordingly, stress concentrations formed at welds also separate.

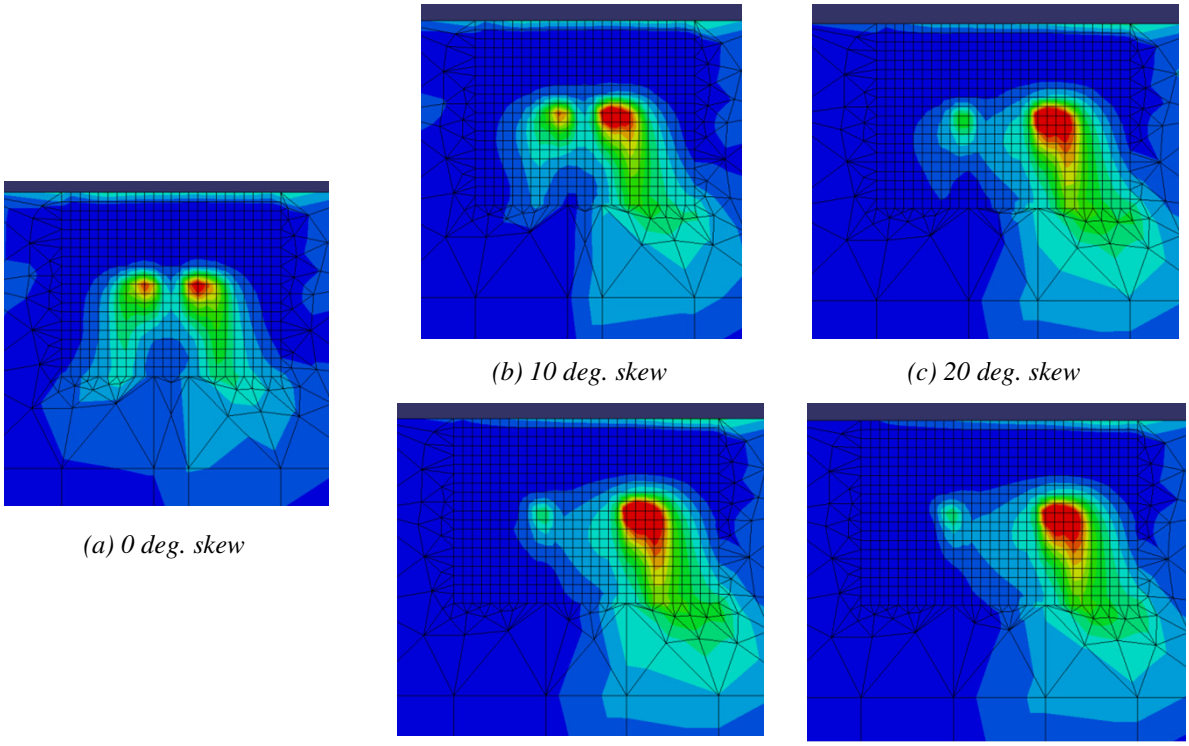

(a) 0 deg. skew

(b) 10 deg. skew

(c) 20 deg. skew

(d) 30 deg. skew

(e) 40 deg. skew

Figure D.2: Effect of skew on web gap stresses

As skew angle increased, more of the stress was concentrated at the weld on the right side of the connection stiffener. This is the side of the cross frame that forms an increasingly large obtuse angle with the girder web. It is interesting to note that the two stress concentrations in the 0 deg. skew bridge are not equal. The stress concentration on the right side is larger because the cross frame itself is not symmetrical. Stress is unequally distributed because the angle framing into the top web gap is connected on the right side of the connection plate. The uneven stress concentrations also show the presence of bending: tensile (red) stress at the right weld and compressive (blue) stress at the left.

D.4: CONCLUSIONS

Distortion-induced fatigue produces a complex, three-dimensional stresses state in the web gap region. Maximum principal and/or von Mises stresses may be used for finite element analysis, but individual directional stresses (in-plane and out-of-plane) must be understood to compare results to experimental studies and previous research. Results of this analysis can be summarized as follows:

- Stress concentration at the web to flange weld is caused primarily by vertical, in-plane stress resulting from relative rotation between the top flange and web.
- All three directional stresses contribute to the stress concentration formed at the connection stiffener to web weld, but longitudinal, in-plane stress has the highest magnitude and is distributed over the largest area.
- As skew angle increases in bridges will cross frames placed parallel to skew angle, stress distribution between the two welds at the connection stiffener to web intersection becomes more uneven. Tensile stress is more concentrated on the side of the connection stiffener forming an obtuse angle with the web.

This study highlights the importance of considering all three directional stresses when evaluating distortion-induced fatigue susceptibility. It also shows bridge inspectors looking for distortion-induced fatigue related cracking in skewed bridges should pay close attention to the side of the bracing forming an obtuse angle with the girder. This is the side of the connection most easily seen.